

Thesis Submitted to the Faculty of the
Virginia Polytechnic Institute & State University
In partial fulfillment of the requirements for the degree of

Master of Science
in
Electrical Engineering

A Nonlinear Technique for Bandwidth Improvement in Narrowband Antennas

Kojo S. Zilevu

Committee Members:
Majid Manteghi, Chair
William A. Davis
Ahmad Safaai-Jazi

April 24, 2012
Blacksburg, Virginia

Keywords: Bandwidth, Narrowband, Antennas, Nonlinear
Copyright 2012, Kojo S. Zilevu

A Nonlinear Technique for Bandwidth Improvement in Narrowband Antennas

Kojo S. Zilevu

(ABSTRACT)

Electrically small, low profile antennas have become the new frontier in wireless communication research. With the pressure to miniaturize wireless communication devices, engineers are turning to small low profile antennas as a way to reduce their antennas and hence their devices.

Ideally, one would also like to at least maintain antenna bandwidth and efficiency while reducing size. However, in theory, antenna performance degrades when it is miniaturized—impedance bandwidth decreases with the reduction in antenna size.

This thesis investigates the possibility of increasing the input impedance bandwidth without enlarging the volume of the antenna. This thesis attempts to break the fundamental tradeoff between antenna size and bandwidth by loading it with a nonlinear element. First, a brief summary of antenna background definitions is presented. Next, the analytical framework of the thesis is presented using a model of a narrowband antenna.

A literature review of various narrowband electrically small antennas is studied, including the pros and cons of the Inverted-F antenna (IFA), Inverted-L antenna (ILA), and the Planar Inverted-F antenna (PIFA). Next, the analysis and the methodology leading to results are discussed and simulated results are presented. Simulated results show that the PIFA is able to achieve a higher bandwidth with a loaded nonlinear element. However, it is difficult to sustain the efficiency of the antenna due to harmonics generated by nonlinearity in the antenna. Results indicate that an increase in nonlinearity tends to generate harmonics which leads to losses in the antenna.

Acknowledgements

I would first like to thank my Heavenly Father and my oldest brother Jesus for the love and discipline throughout the thesis and the opportunity to grow me up in my faith.

Secondly, I would like to thank Dr. Majid Manteghi for being my advisor and serving as my committee chairman as well as funding every semester of my graduate research. This research project would not have been possible without Dr. Manteghi for helping me understand electromagnetics, and antennas both as an undergraduate and graduate student.

Special thanks to Dr. William Davis and Dr. Ahmad Safaai-Jazi for serving on my graduate committee; I would like to thank Dr. Davis for all the advice, suggestions and direction throughout my time working in the Virginia Tech Antenna Group. Speaking of the Virginia Tech Antenna Group, I would like to thank all my colleagues there especially Mohsen for the helping me understand the concept of nonlinearity in antennas.

Finally, I would like to thank my brothers Kwashie and Setor, my cousin Selali as well as my parents Eva and Johnny for their patience, encouragement and support through my time here at Virginia Tech.

Table of Contents

Chapter 1	Introduction.....	1
1.1	Motivation.....	1
1.2	Thesis Outline	1
Chapter 2	Wireless Communication History and Antenna Theory Background.....	3
2.1	Wireless Communication History	4
2.2	Multi-Resonant Single Element Antennas	5
2.3	Fundamental Properties of Small Antennas.....	7
2.3.1	Gain and Directivity.....	7
2.3.2	Input Impedance and Efficiency	7
2.3.3	Reflection Coefficient and Voltage Standing Wave Ratio	8
2.4	Quality Factor and Bandwidth	10
2.5	Breaking the Fundamental Limits of Antennas.....	13
Chapter 3	A Nonlinear Antenna Circuit Model.....	15
3.1	A Narrowband Antenna Model.....	16
3.1.1	Theoretical deviation of Nonlinear Resonator.....	17
3.2	Analytical Solution with Method of Multiple Scales.....	19
3.3	Numerical Algorithms.....	20
3.3.1	Euler Method	21
3.3.2	4 th Order Runge-Kutta Method.....	21
3.4	Numerical Approach with Nonlinearity.....	22
3.5	Numerical Simulation Results.....	26
3.5.1	Case I: Variation in Nonlinear Factor.....	26
3.5.2	Case II: Excitation Bandwidth and Nonlinearity Factor Varied.....	29
3.5.3	Case III: Excitation Amplitude and Nonlinearity Factor Varied	31
Chapter 4	Low Profile Antennas for Wireless Communications	35
4.1	The Inverted-L Antenna.....	36
4.1.1	Frequency Analysis and Radiation Pattern.....	36
4.1.2	Input Impedance.....	37
4.2	The Inverted-F Antenna	38
4.2.1	Frequency Analysis and Input Impedance.....	38
4.3	The Planar Inverted-F Antenna.....	39
4.3.1	Frequency Analysis.....	40
4.3.2	Bandwidth of Planar Inverted-F Antenna.....	41

Chapter 5	Down selection of Low Profile Antenna.....	44
5.1	Linear PIFA Antenna	45
5.2	Simulated Results.....	46
5.2.1	Far-Field Radiation Pattern.....	47
5.3	PIFA Structure Variation on Input Impedance and Bandwidth.....	50
Chapter 6	A Nonlinear Tuned PIFA Antenna	53
6.1	Methodology and Algorithms	54
6.1.1	Antenna Field Simulator and RF Simulator.....	54
6.1.2	Exporting Scattering Parameters in ADS	54
6.1.3	RF Algorithms: Harmonic Balance and LSSP Parameters.....	55
6.2	Nonlinear Antenna Structure.....	58
6.3	Nonlinear Inductor DC Bias Model and Analysis	60
6.4	Simulation Results with 1 st PIFA Structure	62
6.5	Simulation Results with 2 nd PIFA Structure	66
6.6	Concerns using Nonlinearity.....	71
Chapter 7	Conclusions.....	74
7.1	Summary	74
7.2	Contributions.....	75
7.3	Future Work	76

Table of Figures

Figure 2.1 Fundamental Limit Curves of radiation quality factor verses ka for various radiation efficiencies	11
Figure 2.2 Fundamental Limit Curves of Maximum Fraction Bandwidth Percentage verses ka for various radiation efficiencies	12
Figure 3.1 Circuit Model of a Nonlinear Parallel Resonator	16
Figure 3.2 Saturation Curves of Nonlinear Inductor	17
Figure 3.3 Frequency Response Methodology for Nonlinear RLC Resonator.....	23
Figure 3.4 Time and Frequency Domain of Gaussian Function.....	24
Figure 3.5 Nonlinear Resonator with its Differential Equation.....	25
Figure 3.6 Nonlinear RLC Input Impedance Methodology.....	25
Figure 3.7 Comparison of Input impedance magnitude response for a system modeled in Eq(3.25) with nonlinearity ($\alpha = 0.12$). Other parameters defined in Table 3.1	27
Figure 3.8 Comparison of Input impedance magnitude response for a system modeled in Eq(3.25) with nonlinearity ($\alpha = 0.14$). Other parameters defined in Table 3.1	28
Figure 3.9 Comparison of Input impedance magnitude response for a system modeled in Eq(3.25) with nonlinearity ($\alpha = 0.5$). Other parameters defined in Table 3.1	28
Figure 3.10 Comparison of Input impedance magnitude response for a system modeled in Eq (3.25) with nonlinearity ($\alpha = 0.12$). Other parameters defined in Table 3.3.....	29
Figure 3.11 Comparison of Input impedance magnitude response for a system modeled in Eq (3.25) with nonlinearity ($\alpha = 0.14$). Other parameters defined in Table 3.3.....	30
Figure 3.12 Comparison of Input impedance magnitude response for a system modeled in Eq(3.25) with nonlinearity ($\alpha = 0.5$). Other parameters defined in Table 3.3.	30
Figure 3.13 Comparison of Input impedance magnitude response for a system modeled in Eq with nonlinearity ($\alpha = 0.12$). Other parameters defined in Table 3.5.	32
Figure 3.14 Comparison of Input impedance magnitude response for a system modeled in Eq with nonlinearity ($\alpha = 0.14$). Other parameters defined in Table 3.5.	32
Figure 3.15 Comparison of Input impedance magnitude response for a system modeled in Eq with nonlinearity ($\alpha = 500,000$). Other parameters defined in Table 3.5.	32
Figure 4.1 The Inverted-L Antenna geometry	36
Figure 4.2 The Inverted- F Antenna	38
Figure 4.3 The Planar Inverted-F Antenna	40
Figure 5.1 Planar Inverted-F Antenna (1 GHz)	45
Figure 5.2 Reflection Coefficient versus frequency of planar inverted-F antenna.....	46
Figure 5.3 Input Impedance versus frequency of planar inverted-F antenna	47
Figure 5.4 3D Total Radiation Pattern of PIFA	48
Figure 5.5 Calculated Radiation Patterns, $E_{\theta}(\varphi = 0^{\circ})$ and $E_{\theta}(\varphi = 90^{\circ})$	48
Figure 5.6 Calculated Radiation Patterns, $E_{\theta}(\theta = 90^{\circ})$ and $E_{\phi}(\theta = 0^{\circ})$	49
Figure 5.7 Input Impedance verses frequency for PIFA with various separation distance	50
Figure 5.8 Impact of dimension S on reflection coefficient	51
Figure 5.9 Impact of PIFA height on reflection coefficient.....	52
Figure 6.1 ADS Two-Port Antenna Simulation.....	55
Figure 6.2 Methodology in Nonlinear Antenna Design.....	55

Figure 6.3 Harmonic Balance Simulation Steps	56
Figure 6.4 Current Density Plot of PIFA Antenna	59
Figure 6.5 Inductance vs. DC Bias Current	60
Figure 6.6 Nonlinear Loading on PIFA: results generated using HFSS and ADS	62
Figure 6.7 Input Impedance of Nonlinear Antenna with different nonlinearities.....	63
Figure 6.8 Voltage Standing Wave Ratio (VSWR) of Nonlinear Antenna with different nonlinearities	64
Figure 6.9 Comparison of Linear PIFA vs a Tuned Nonlinear PIFA.....	65
Figure 6.10 Reflection Coefficient (S_{11}) of 1.4 GHz PIFA Structure.....	66
Figure 6.11 Input Impedance of 1.4 GHz PIFA Structure.....	67
Figure 6.12 Reflection Coefficient of nonlinear loading on 1.4GHz PIFA: results generated using HFSS and ADS	68
Figure 6.13 Input Impedance of nonlinear loading on 1.4 GHz PIFA: results generated using HFSS and ADS	69
Figure 6.14 VSWR of nonlinear loading on 1.4 GHz PIFA: results generated using HFSS and ADS.....	70
Figure 6.15 Input Power and Radiated Power at Harmonics of the Fundamental Frequency.....	71

List of Tables

Table 2.1 Some Wireless Communication Bands.....	5
Table 3.1 Parameters used to simulate nonlinear resonator modeled in Eq. (3.25).....	27
Table 3.2 Input Impedance Bandwidth of RLC circuit with various nonlinear factors.....	28
Table 3.3 Parameters used to simulate nonlinear resonator modeled in Eq. (3.25).....	29
Table 3.4 Input Impedance Bandwidth of RLC circuit with various nonlinear factors.....	31
Table 3.5 Parameters used to simulate nonlinear resonator modeled in Eq. (3.25).....	31
Table 3.6 Input Impedance Bandwidth of RLC circuit with various nonlinear factors.....	33
Table 5.1 Dimensions for 1 GHz PIFA: Geometry layout is shown in Figure 5.1.....	46
Table 6.1 Nonlinear Antenna Dimensions.....	58
Table 6.2 Summary of Results Generated in Figure 6.6.....	64
Table 6.3 Comparison of Linear PIFA vs a Tuned Nonlinear PIFA.....	65
Table 6.4 Summary of results generated in Figure 6.14.....	70

Chapter 1 Introduction

1.1 Motivation

The electronic world faces a tremendous burden to miniaturize its handheld wireless devices.

The demand to reduce wireless electronic devices comes with another need to reduce its antennas. Theoretically, reducing the size of small antennas comes with an added tradeoff— a reduction in their function capabilities such as bandwidth and impedance matching. Although a single antenna can be designed to cover multiple bands, it comes with an added complexity.

Typically, there is a tradeoff between covering the bandwidth of one frequency band verse another. The focus of this thesis was to explore the possibility of using a nonlinear inductor as a loading mechanism on electrically small antennas for size reduction as well as bandwidth improvement. The goal is to increase the narrow bandwidth of the antenna by introducing a nonlinear element to the antenna structure. The Planar Inverted-F Antenna (PIFA) was chosen as a candidate antenna to load the nonlinear element because its structure diversity.

1.2 Thesis Outline

The outline for the thesis is as follows. Chapter 2 covers the basic concepts of antennas and gives a history of wireless communication systems. A literature review linking the radiation quality factor to the antennas size is also discussed. The chapter ends with the possibility of increasing the antennas bandwidth by defeating Chu's criteria with a nonlinear inductor. Chapter 3 models

the input impedance of a nonlinear antenna as a parallel narrowband resonator with a nonlinear inductor and simulation results are presented. Chapter 4 discusses various candidate low profile narrowband small antennas such as the Planar Inverted – F Antenna for nonlinear loading. A more in depth study is done on the PIFA using the EM Simulator HFSS in Chapter 5. Finally, Chapter 6 presents the simulation results and the methods used to acquire them. Chapter 7 summaries the overall thesis and concludes with possible future work.

Chapter 2 Wireless Communication History and Antenna Theory Background

The growth of wireless communication systems is evident in many handheld devices today. Smart phones now can support multiple cellular bands and have the ability to be GPS receivers, use Wi-Fi and Bluetooth. Other devices such as the iPads and iPods have similar features. This chapter gives a brief history of cellular phones, GPS and WLAN. Section 2.2 discusses the advantages and disadvantages of multi-resonant single element antenna systems. The rest of the Chapter gives an overview of basic antenna theory concepts and finally Section 2.5 lays the foundation for the thesis.

2.1 Wireless Communication History

Cellular networks make up a huge portion of wireless communications in the United States. After the first commercially automated cellular network began in 1979 by the Japanese company NTT, more countries began to follow. In 1983, Motorola unveiled the first portable cellular phone to the world. By that time the FCC had allocated the Advanced Mobile Phone Service (AMPS) band for AT&T, but it took 15 years for cellular phones to appear on the market [1].

By the early 1990s, cellular phones were part of the Global System for Mobile communications (GSM) and Code Division Multiple Access (CDMA) bands [1]. Soon, digital mobile networks replaced their analog counterparts. As phones were made more portable, the reduction in their size made it more appealing to consumers. After a few years, the third generation cellular network was opened to the market with features that gave cellular phones more capabilities such as text messaging and faster data speeds.

The evolution of a wireless mobile telephony has inspired the growth of other wireless technology such as the Global Positioning System (GPS). It was first introduced as a combination of satellites created and maintained by the US Department of Defense (DoD). The system was originally established on 24 satellites (21 operational) which were put in space by the United States for military defense positional location purposes. Now, the system provides civilian users with highly accurate position, velocity and time information anywhere around the globe.

Another widely used wireless communication technology is the wireless local area network (WLAN). WLAN allows users to connect to a wired local area network via radio or infrared signals. It provides wireless network communication over short distances by linking a number of access points to a wired LAN backbone [2]. With access points, users can now

connect wirelessly from a range of about 50m to the LAN service. 802.11 was the first basic standard defined for WLAN communications working in the 2.4GHz spectrum. Numerous revisions have been made to the standard and it now provides up to 150 Mbit/s data rates in the 2.4 GHz and 5GHz ISM bands. Bluetooth which offers short range (10m) communication between devices also operates around the same band at 2.4 GHz.

2.2 Multi-Resonant Single Element Antennas

The advances in wireless technology have now made it possible for a single device to include various features such as GPS, WLAN and Bluetooth. For instance, sophisticated cell phones are required to have multiple cellular frequency bands and include GPS, WLAN and Bluetooth integration as well. These frequency bands typically require bandwidth to operate efficiently.

Table 2.1 shows some wireless communication bands and their required bandwidth.

Table 2.1 Some Wireless Communication Bands

<i>Band Name</i>	<i>Transmit Frequency (MHz)</i>	<i>Receive Frequency (MHz)</i>	<i>Total Bandwidth (MHz)</i>	<i>Bandwidth Percentage</i>
GSM 800	824- 849	869-894	70	8.1%
GSM 1800 (DCS 1800)	1710-1785	1805-1880	170	10.6%
GSM 1900 (PCS 1900)	1850-1910	1930-1990	140	7.3%
UMTS	1885-2025	2110-2200	315	15.5%
WLAN	2400-2483.5		83.5	3.5%
Bluetooth	2400-2500		100	4.1%
GPS	N/A	1565.42 – 1585.42	20	1.3%

With a single handheld device requiring multiple antennas for various frequency bands and reduction in size, antenna engineers face a challenge to further reduce the antenna size as well as increase the its operating bandwidth. The demand to miniaturize cellular phones comes

with a need to miniaturize its antenna element. A unique way of reducing the number of antennas is to use multi-resonant single element antennas. By integrating multiple frequencies bands into one antenna, space as well as data speed and errors are reduced.

The disadvantage of multi-resonant antennas is the tradeoff of efficiency and bandwidth in one frequency band over another. These diversity or smart antennas also have their limitations in terms of bandwidth. Typical low profile antennas such as Planar Inverted-F Antennas (PIFAs), Inverted-L Antennas (ILA) offer around 6% bandwidth without any modifications. To solve this problem, smart antennas have to extend beyond their fundamental limits to cover multiple frequency bands. Section 2.3 reviews the fundamental properties and limits of small antennas.

2.3 Fundamental Properties of Small Antennas

2.3.1 Gain and Directivity

The directivity is the ratio of power density in the direction of the pattern maximum to the average power density at the same distance from the antenna. In other words, it measures the ratio of the radiation intensity in a specific direction to the average radiation intensity [3]. While directivity simply measures the ability of an antenna to focus energy in a particular direction when transmitting or receiving, Gain is measures how much of the directivity is left after losses are accounted for. Therefore, the relationship between gain and directivity can be written as

$$G = e_r D \quad (2.1)$$

where e_r is the radiation efficiency. Section 2.3.2 presents more in-depth overview on radiation efficiency.

2.3.2 Input Impedance and Efficiency

Input Impedance of an antenna is defined as the ratio of voltage to current at its terminals. The input impedance of an antenna is useful in determining the efficiency. It is generally also dependent of the frequency, at which the antenna is operating— that is, at different frequencies, the input impedance of the antenna will change. For an electrically small antenna, the input impedance can be written as

$$Z_{ant}(\omega) = R_a(\omega) + jX_a(\omega) \quad (2.2)$$

where $R_a(\omega)$ and $X_a(\omega)$ are the input resistance and reactance respectively. Furthermore, small antennas either behaves like a parallel or series RLC circuit depending on the frequency derivative of its reactance, $X'_a(\omega)$. If the reactance derivative is greater than zero at resonance,

than the antenna behaves like a series RLC circuit [4]. In addition, its reactance will approach $-\infty$ as $\omega \rightarrow 0$.

The radiation efficiency for antennas behaving like a series RLC circuit is given by

$$e_r(\omega) = \frac{R_r(\omega)}{R_a(\omega)} = \frac{R_r(\omega)}{R_r(\omega) + R_l(\omega)} \quad (2.3)$$

where $R_r(\omega)$ is the radiation resistance in series with the loss associated with the antenna, $R_l(\omega)$.

Examples of small antenna that behave like series RLC circuits from an impedance viewpoint are dipole and monopole antennas.

On the other hand the radiation efficiency for antennas behaving like a parallel RLC circuit is given in Equation (2.4) where the antenna loss is in parallel with its radiation resistance.

$$e_r(\omega) = \frac{R_a(\omega)}{R_r(\omega)} = \frac{R_l(\omega)}{R_r(\omega) + R_l(\omega)} \quad (2.4)$$

The input impedance of such an antenna will be inductive before resonance and a capacitive after resonance. Small antennas have this behavior when there is a DC short between the antenna structure and the ground plane. Examples include slot antennas, patch antennas and planar-inverted-F antennas (PIFAs).

2.3.3 Reflection Coefficient and Voltage Standing Wave Ratio

At high frequencies, scattering parameters are used to describe the power flow of devices. The reflection coefficient is the same as the S_{11} of the antenna. The reflection coefficient measures the how much power passes through to the antenna compared to how much power is directed at

the port. The power directed at the antenna's port is called the incident wave and the power that returns to the source is called the reflected wave. The equation for the reflection coefficient is given as

$$\Gamma(\omega) = S_{11}(\omega) = \frac{V_{reflected}}{V_{incident}} = \frac{Z_{ant}(\omega) - Z_o}{Z_{ant}(\omega) + Z_o} \quad (2.5)$$

where Z_o is the characteristic impedance of the transmission line connecting source to the antenna. The standard impedance use is 50 ohms, but it can be different based on what the antenna is used for. A completely matched antenna will have a reflection coefficient of 0, which means the impedance of the transmission line or port is equal to the antenna's input impedance. Therefore, at resonance, it is desirable match the antenna input impedance to the transmission line or port impedance.

Another important definition that shows how match an antenna is to the source is the voltage standing wave ratio (VSWR), which is a ratio of the maximum to minimum voltage when the incident wave mixes with the reflected signal at the antenna node. Its definition is related to the reflection coefficient and can be expressed as

$$VSWR = s = \frac{1 + |\Gamma(\omega)|}{1 - |\Gamma(\omega)|} \quad (2.6)$$

So an antenna with a VSWR of 2:1 means the maximum voltage is twice as much as the minimum voltage and has a return loss of 10dB. Although it is desirable to have a well match antenna; it doesn't necessarily mean that the antenna is efficient. The VSWR of an antenna also has some relationship to the bandwidth and quality factor.

2.4 Quality Factor and Bandwidth

An antenna is considered electrically small when the minimal sphere ka , that encloses the antenna less than or equal to 1. k is the wave number which is defined as $2\pi/\lambda$ and a is the maximum radius the antenna covers. Using this definition of electrically small, the radiation quality factor Q of an antenna can be approximated. In fact, Wheeler [5] and Chu [6] were the first to show that the radiation Q of antenna was related to the antenna's physical size and wavelength. Chu [6] computed the radiation Q as

$$Q = \begin{cases} \frac{2\omega W_e}{P_{rad}} & \text{when } W_e > W_m \\ \frac{2\omega W_m}{P_{rad}} & \text{when } W_m > W_e \end{cases} \quad (2.7)$$

In equation (2.7), W_e and W_m are the average stored electric and magnetic energy outside the sphere of the antenna. P_{rad} is the radiated power from the antenna and ω is the frequency in radians per second. MacLean [7] expanded on Chu's work and found that the radiation Q can be approximated as

$$Q_{Exact} = e_r \left(\frac{1}{(ka)^3} + \frac{1}{ka} \right) \quad (2.8)$$

From this equation, an antenna with low radiation efficiency will have a lower Q and hence a higher bandwidth even though it isn't efficient. Therefore the radiation efficiency has to be examined to see if the antenna has a wider bandwidth because of its "lossy" characteristics. In such a case, the antenna is inadequate to be used in applications where efficiency is of importance.

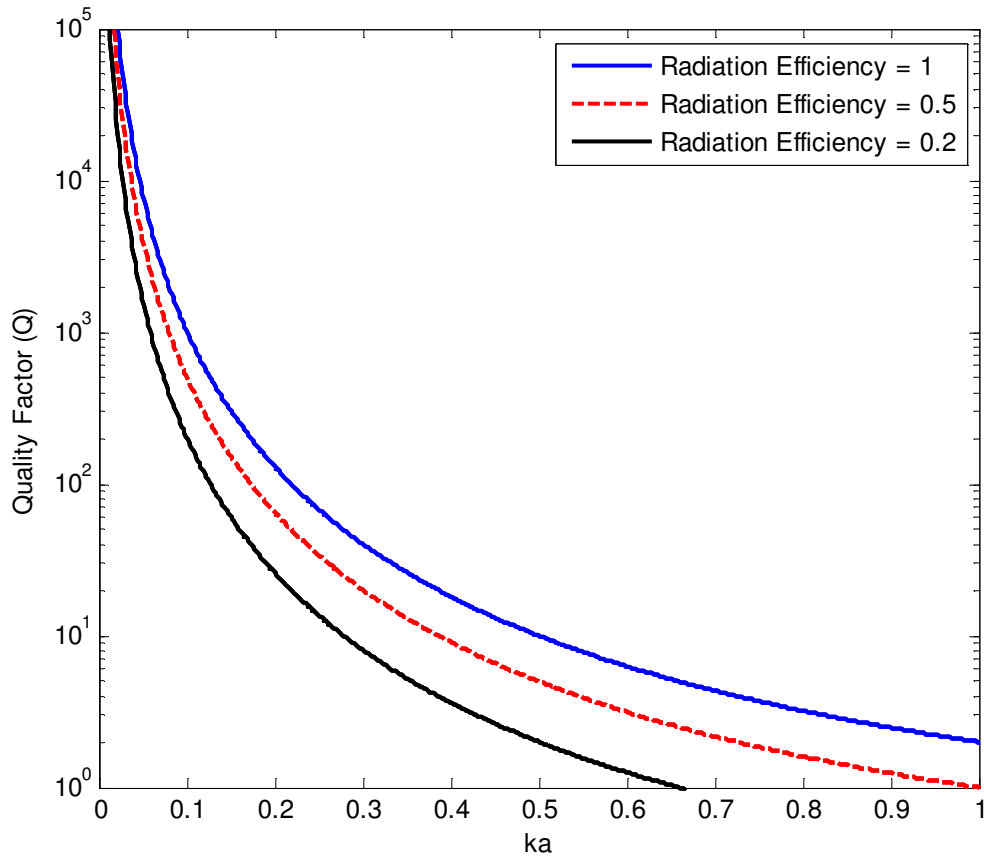


Figure 2.1 Fundamental Limit Curves of radiation quality factor versus ka for various radiation efficiencies

The bandwidth of an antenna, which measures the frequencies where the antenna can transmit or receive signals efficiently, is related to the quality factor of the antenna. The normalized 3dB bandwidth is defined as [8]

$$BW = \frac{f_u - f_l}{f_c} \cong \frac{1}{Q_{BW}} \quad (2.9)$$

where f_u and f_l are upper and lower frequencies describing the antennas transmit or receiver range. f_c is the center frequency of the operating antenna and Q_{BW} is the radiation quality factor.

The normalized 3dB bandwidth definition assumes a VSWR =1, but that's not the standard used.

An antenna's bandwidth is often defined in terms of the minimum VSWR bandwidth. With the minimum VSWR is taken into account, the bandwidth is defined as

$$BW_{VSWR} \cong \frac{VSWR - 1}{Q_{BW} \sqrt{VSWR}} \cong \frac{s - 1}{Q_{BW} \sqrt{s}} \quad (2.10)$$

Substituting Equation (2.8) into (2.10), the maximum fractional bandwidth is defined as

$$FBW = \frac{1}{Q_{Exact}} \cong \frac{1}{e_r} \left(\frac{(ka)^3}{[1 + (ka)^2]} \right) \cong \frac{(ka)^3}{e_r} \frac{s - 1}{\sqrt{s}} \quad (2.11)$$

And when the standard VSWR = 2, Equation 2.11 reduces to

$$FBW_{VSWR=2} \cong \frac{1}{\sqrt{2}} \frac{(ka)^3}{e_r} \quad (2.12)$$

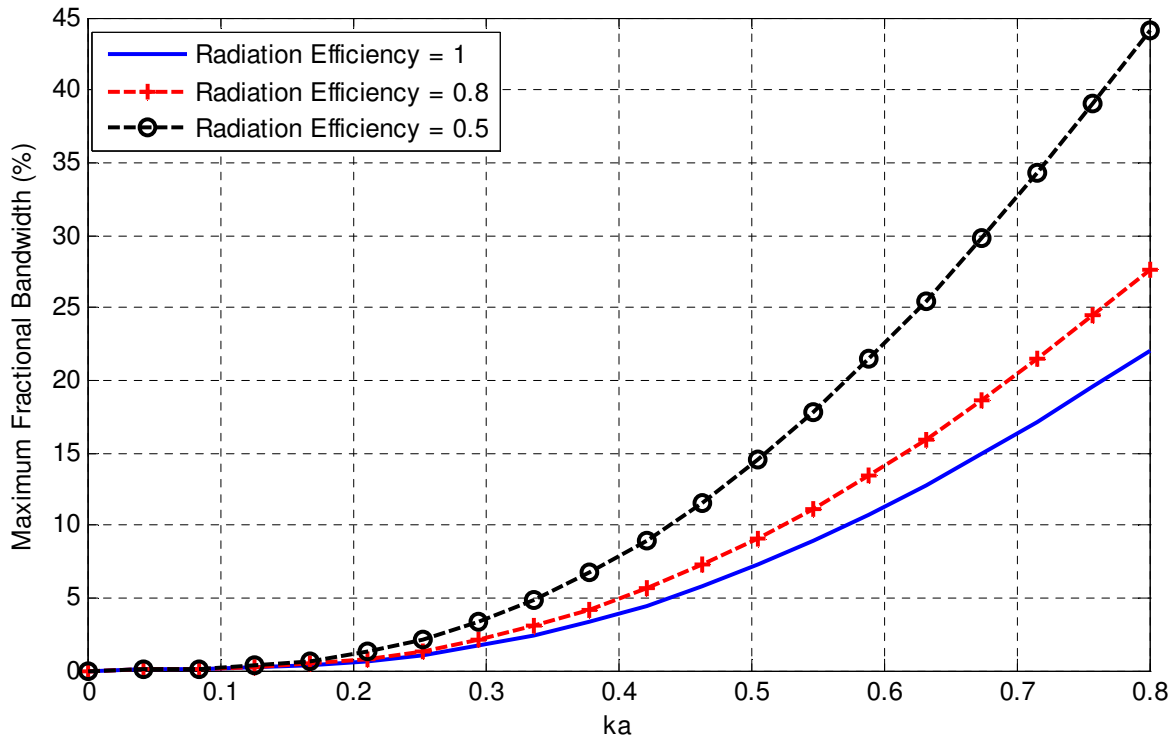


Figure 2.2 Fundamental Limit Curves of Maximum Fraction Bandwidth Percentage versus ka for various radiation efficiencies

2.5 Breaking the Fundamental Limits of Antennas

As seen in the previous section, small antennas have a fundamental limit on bandwidth based on the size of the antenna — the smaller the size of an electrically small antenna, the higher the quality factor and hence narrower bandwidth. Numerous techniques have been proposed to reduce the quality factor of the antenna, but it comes with a trade off in complexity and size. So there is a limit on the achievable bandwidth a small antenna can have based on Chu's quality factor equation. Chu's limit [6] is based on a couple of assumptions: the antenna radiates on a single mode, is linear and time invariant. So in order to further increase the antenna's bandwidth beyond its theoretical limits, the antenna has to be nonlinear, time variant or have multi frequency modes. Chapter 2 shows how to achieve a broader bandwidth by inserting a nonlinear element inside the antenna structure.

References

- [1] “History of Cell Phones,” Internet: <http://www.tech-faq.com/history-of-cell-phones.html>, Nov. 11, 2001 [Dec. 2, 2011].
- [2] T.Franklin, “Wireless Local Area Networks Technical Report,” Internet: <http://www.jisc.ac.uk/media/documents/publications/wirelesslantechrep.pdf>, Aug.26, 2002 [Dec. 2, 2011].
- [3] W.L Stutzman and G.A. Thiele, *Antenna Theory and Design*, New York: John Wiley & Sons, Inc., 1998
- [4] David A. Sanchez-Hernandez. “Fundamental Antenna Properties Definitions” in *Multiband integrated antennas for 4G terminals*, 1st Edition, Spain: Artech House, Aug 2008
- [5] H. A. Wheeler, “Fundamental Limitations of Small Antennas,” *Proc. IRE*, 35, December 1947, pp. 1479 – 1484.
- [6] L. J. Chu, “Physical Limitations of Omni-Directional Antennas,” *J. Appl. Phys.*, 19, December 1948, pp 1163-1175.
- [7] J.S Maclean, “A Re-Examination of the Fundamental Limits on the Radiation Q of Electrically Small Antennas,” *IEEE Trans. Ant. Prop.*, vol. AP-44, no.5, May 1996, pp. 672-676
- [8] R.C Hansen, “Fundamental limitations in antennas,” *Proceedings of the IEEE*, 69, 170-182. (1981)

Chapter 3 A Nonlinear Loaded Antenna Circuit

Model

Ferromagnetic materials have the unique property of saturating as current increases through its core. This characteristic makes it nonlinear and therefore can be integrated into electrical small antennas to make it nonlinear in order to break Chu's limit. This chapter presents a foundation for the theory by first showing how the input impedance of a narrowband antenna can be modeled into a lumped circuit in Section 3.1. Section 3.2 shows the model and derivation of a proposed RLC circuit with a nonlinear inductor as a ferromagnetic material. Section 3.3 explains the analytical solution and numerical setup for the Nonlinear RLC circuit and finally Section 3.4 displays the numerical simulation results for bandwidth enhancement.

3.1 A Narrowband Antenna Model

Small antennas such as dipoles and monopoles which are considered narrowband for low profile wireless applications can be modeled as a series RLC circuit from an impedance perspective [1]. This is due to the fact that the input impedance of most antennas can be modeled as some sort of resonator around its resonant frequency. Narrowband antennas used in cellular phones such as Inverted-F and Planar Inverted-F antennas can be modeled as a parallel RLC circuit around its resonant frequency. Such antennas have a DC short somewhere in the antenna structure which connects the radiating element to ground, plus making them behave like parallel RLC circuits from an impedance perspective [1].

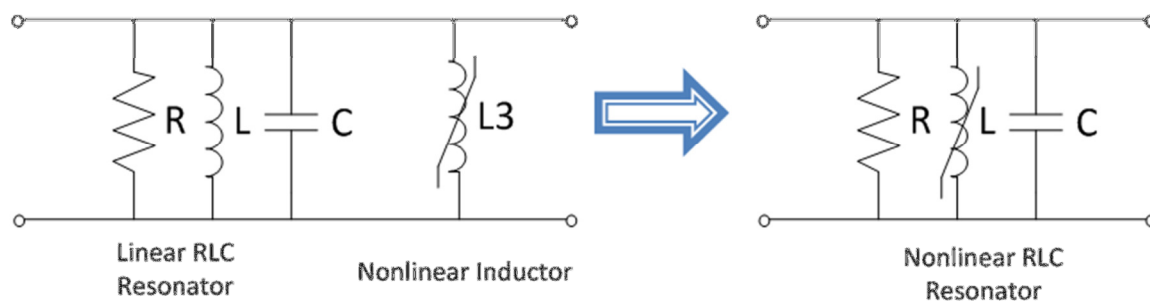


Figure 3.1 Circuit Model of a Nonlinear Parallel Resonator

Moreover, information like the antenna bandwidth and quality factor can be integrated into the parallel RLC circuit. With a lumped circuit model, modifications and additions can be made into the RLC circuit to study how the bandwidth characteristics of the antenna changes. In this chapter, a nonlinear inductor is attached to the RLC circuit for bandwidth enhancement. To simplify the circuit, the external nonlinear inductor is combined with the linear antenna RLC resonator to form the equivalent nonlinear circuit model shown in Figure 3.1

3.1.1 Theoretical deviation of Nonlinear Resonator

For this section, a derivation of the nonlinear resonator is presented using basic circuit theory and a nonlinear inductor model. Because of the nonlinearity in the inductor, the voltage drop across the inductor is not proportional to the rate of change of current. This occurs when the core permeability becomes excitation dependent; the current through coil becomes high, causing the magnetic core to saturate.

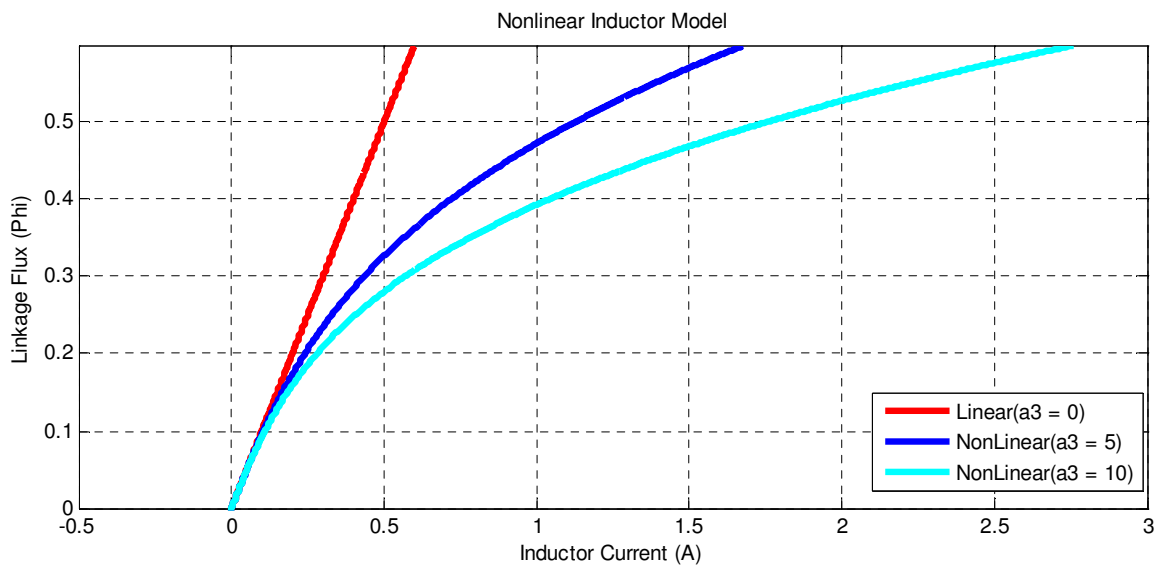


Figure 3.2 Saturation Curves of Nonlinear Inductor

The current through the nonlinear inductance is

$$i_L = \frac{\varphi}{L} + a_3 \varphi^3 \quad (3.1)$$

where φ is the magnetic linkage flux and i_L is the current through the inductor. Figure 3.2 shows how nonlinearity changes the current across the inductor. To predict the behavior of the circuit,

we first have to find the relationship between the input voltage and current. From Kirchhoff's voltage law, the input voltage is

$$v(t) = v_L = v_C = v_R \quad (3.2)$$

where v_L, v_C, v_R are the voltages across the inductor, capacitor and resistor respectively. To derive the differential equation the voltage must satisfy, we sum up the current in the circuit

$$i(t) = i_L + i_C + i_R \quad (3.3)$$

where i_L, i_C, i_R are the currents across the inductor, capacitor and resistor respectively. We can now replace the inductor current by its nonlinear current seen in Equation (3.1) and also write the current across the resistor and capacitor as a function of the input voltage.

$$i(t) = C \frac{dV}{dt} + \frac{V}{R} + \frac{\varphi}{L} + a_3 \varphi^3 \quad (3.4)$$

Furthermore, the voltage across the inductor is the rate of change of magnetic flux over time:

$$V = \frac{d\varphi}{dt} \quad (3.5)$$

We now write the differential equation as a function of the magnetic flux across the inductor.

Combing Equation (3.4) with Equation (3.5), a differential equation which describes the circuit is

$$\frac{d^2\varphi}{dt^2} + \frac{1}{RC} \frac{d\varphi}{dt} + \frac{\varphi}{LC} + \frac{a_3\varphi^3}{C} = \frac{I_o \cos(\omega t)}{C} \quad (3.6)$$

If we define $\omega_o^2 = \frac{1}{LC}$, $\alpha = \frac{a_3}{C}$, $F = \frac{I_o}{C}$, $d = \frac{1}{RC}$, the equation becomes

$$\frac{d^2\varphi}{dt^2} + d \frac{d\varphi}{dt} + \omega_o^2 \varphi + \alpha \varphi^3 = F(t) = F \cos(\omega t) \quad (3.7)$$

3.2 Analytical Solution with Method of Multiple Scales

Equation (3.7) can be solved using the perturbation theory. However, with perturbation, secular terms — terms growing without bound — make the approximation grow linearly in time. Also, a straightforward expansion using the perturbation theory causes terms with denominators that are very small. Using the method of multiple scales technique, we can express the general solution in terms of different time scales as follows

$$\varphi(t; \varepsilon) = \varphi_0(T_0, T_1) + \varepsilon \varphi_1(T_0, T_1) + \dots \quad (3.8)$$

where $T_n = \varepsilon^n t$ is a small scale and a higher order of n yields a more accurate solution. For this solution, only two time scales $T_0 = t$ and $T_1 = \varepsilon t$ are used. The input signal can be expressed in terms of T_0 and T_1 as

$$F(t) = \varepsilon F \cos(\omega_o T_0 + \sigma T_1) \quad (3.9)$$

Substituting Equation (3.8) and (3.9) into Equation (3.7) and equating the coefficients of ε^0 and ε on both sides, we come up with the expressions

$$D_o^2 \varphi_o + \omega_o^2 \varphi_o = 0 \quad (3.10)$$

$$D_o^2 \varphi_1 + \omega_o^2 \varphi_1 = -2D_o D_1 \varphi_o - 2dD_o \varphi_o - \alpha \varphi_o^3 + \varepsilon f \cos(\omega_o T_0 + \sigma T_1) \quad (3.11)$$

where $D_n = \frac{\partial}{\partial T_n}$. The solution to Equation (3.10) can be found and then substituted into

Equation (3.11) to find its solution. The general solution to Equation (3.10) is

$$\varphi_o = A(T_1) e^{(i\omega_o T_0)} + \bar{A}(T_1) e^{(-i\omega_o T_0)} \quad (3.12)$$

where A and \bar{A} are complex amplitudes and their conjugates, respectively. To find $A(T_1)$, we eliminate the secular terms from φ_1 . Equation (3.13) is substituted into (3.12) and we get

$$D_o^2 \varphi_1 + \omega_o^2 \varphi_1 = -[2i\omega_o (A'+dA) + 3\alpha A^2 \bar{A}]e^{(i\omega_o T_o)} - \alpha A^3 e^{(3i\omega_o T_o)} + 0.5Fe^{[i(\omega_o T_o + \sigma T_1)]} + cc \quad (3.13)$$

Rearranging Equation (3.13) to solve for A , we have

$$-2i\omega_o (A'+dA) + 3\alpha A^2 \bar{A} - 0.5fe^{[i(\sigma T_1)]} = 0 \quad (3.14)$$

and the solution is

$$A = 0.5ae^{i(\beta)} \quad (3.15)$$

where a and β are real and can be separated into real and imaginary parts.

$$a' = -da + \frac{1}{2} \frac{f}{\omega_o} \sin(\sigma T_1 - \beta) \quad (3.16)$$

$$a\beta' = \frac{3}{8} \frac{\alpha}{\omega_o} a^3 - \frac{1}{2} \frac{f}{\omega_o} \cos(\sigma T_1 - \beta) \quad (3.17)$$

Now, we can finally substitute Equation (3.15) into (3.12) to yield an approximate solution as

$$\varphi = a \cos(\omega_o t + \beta) + O(\varepsilon) \quad (3.18)$$

3.3 Numerical Algorithms

The Multiple Scale technique is excellent in determining an approximate analytical solution for nonlinear differential equations, but is unreliable with strong nonlinearities. Another setback in applying perturbation techniques is that it requires a small parameter to be artificially injected into the equation [2]. For simulation purposes, the approximate solution to the nonlinear resonator utilizes the Runge-Kutta (RK) methods, and not the multiple scale method. The Runge-Kutta methods are basically implicit and explicit iterative methods for approximating solutions for the differential equations such as the nonlinear resonator.

3.3.1 Euler Method

Before jumping into the Runge-Kutta Method, let's briefly explain one of the more simple and popular numeric ways of approximating differential equations. The Euler method is written as

$$y_{n+1} = y_n + hf(x_n, y_n) \quad (3.19)$$

which evaluates a solution from x_n to x_{n+1} until it approaches $x_n + h$. The derivative at the starting point of each interval is used to determine a solution through an interval h which leads to a step error of only one power of h . There are two main reasons why the Euler Method is impractical for ODEs. First, it is not very accurate when compared to other methods such as the Runge-Kutta and second, it is unstable [3].

3.3.2 4th Order Runge-Kutta Method

To improve the Euler method, the 4th order Runge-Kutta method adds two steps at the midpoint of each interval. With two additional steps, one can calculate the actual step across the whole interval. The algorithm used is defined as:

$$\begin{aligned} k_1 &= hf(x_n, y_n) \\ k_2 &= hf\left(x_n + \frac{1}{2}h, y_n + \frac{1}{2}k_1\right) \\ k_3 &= hf\left(x_n + \frac{1}{2}h, y_n + \frac{1}{2}k_2\right) \\ k_4 &= hf(x_n + h, y_n + k_3) \\ y_{n+1} &= y_n + \frac{k_1}{6} + \frac{k_2}{3} + \frac{k_3}{3} + \frac{k_4}{6} + O(h^5) \end{aligned}$$

which uses four slopes to evaluate the solution. Each of the slopes estimates the size of the vertical jump across the specific width of solution interval. k_1 uses the Euler's method and k_4

uses the slope at the right end interval. k_2 and k_3 estimate the slope at the midpoint. Notice that greater weight is given to the slopes at the midpoint. One of the advantages of the Runge-Kutta method is that the error percent is on the order of h^5 . The Runge-Kutta algorithm will be employed through the rest of the chapter in solving the nonlinear circuit model.

3.4 Numerical Approach with Nonlinearity

With linear circuits, finding the frequency response involves transforming the circuit components directly to the frequency domain via Laplace Transform. However, because nonlinearity in the circuit generates harmonics, a better approximation will be so solve the circuit in time domain using the Runge-Kutta algorithm and then convert it to the frequency domain using the Fourier Transform. The Fourier Transform states that a continuous signal $x(t)$ can be mapped into series of frequencies with relative amplitudes and phases that compose the time series. The formula used is

$$X(f) = \int_{-\infty}^{\infty} x(t) e^{-i2\pi f t} dt \quad (3.20)$$

For a discrete data $x_T(nt_s)$ of length T , the Discrete Fourier Transform is

$$X_f[l] = \frac{1}{N} \sum_{n=0}^{N-1} x_T(nt_s) e^{-2\pi i l \frac{n}{N}} \quad (3.21)$$

where t_s is the sampling time, $n = 0, 1, 2, \dots, N - 1$ and $l = 0, 1, 2, \dots, N - 1$. Hence the frequency response of a nonlinear RLC circuit can be found using the Discrete Fourier Transform. First, the time domain solution is approximated using the Runge-Kutta numerical method. With the time domain solution now in discrete points, the Discrete Fourier Transform

can be applied to obtain the frequency response solution. The Figure 3.3 shows a summary of the steps in finding the frequency response solution.

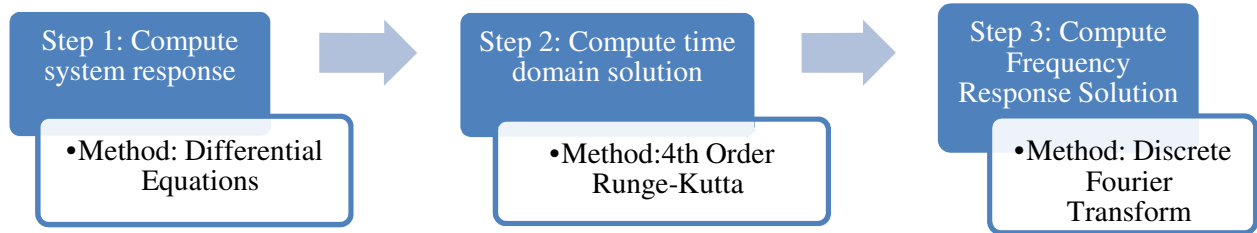


Figure 3.3 Frequency Response Methodology for Nonlinear RLC Resonator

To determine how nonlinearity changes the bandwidth of the signal, we will introduce a signal with a specific bandwidth in the frequency domain. A sinusoidal signal cannot be used here because it only gives a solution corresponding to the magnitude of one particular frequency. So to investigate how the nonlinear inductor alters a signal, a Gaussian Pulse current signal defined as

$$G_P(t) = \frac{1}{\sqrt{2\pi}\sigma} e^{-\frac{t^2}{2\sigma^2}} \quad (3.22)$$

with its Fourier transform

$$G_P(f) = e^{-\frac{\sigma^2 \omega^2}{2}} \quad (3.23)$$

is used to excite the nonlinear circuit model. The Gaussian Pulse has a unique property where its frequency domain bandwidth can widen by altering its time domain signal. In other words, we can now perform a frequency sweep similar to the Laplace Transform by widening the Gaussian signal in the frequency domain. Figure 3.4 has been provided to show this relationship.

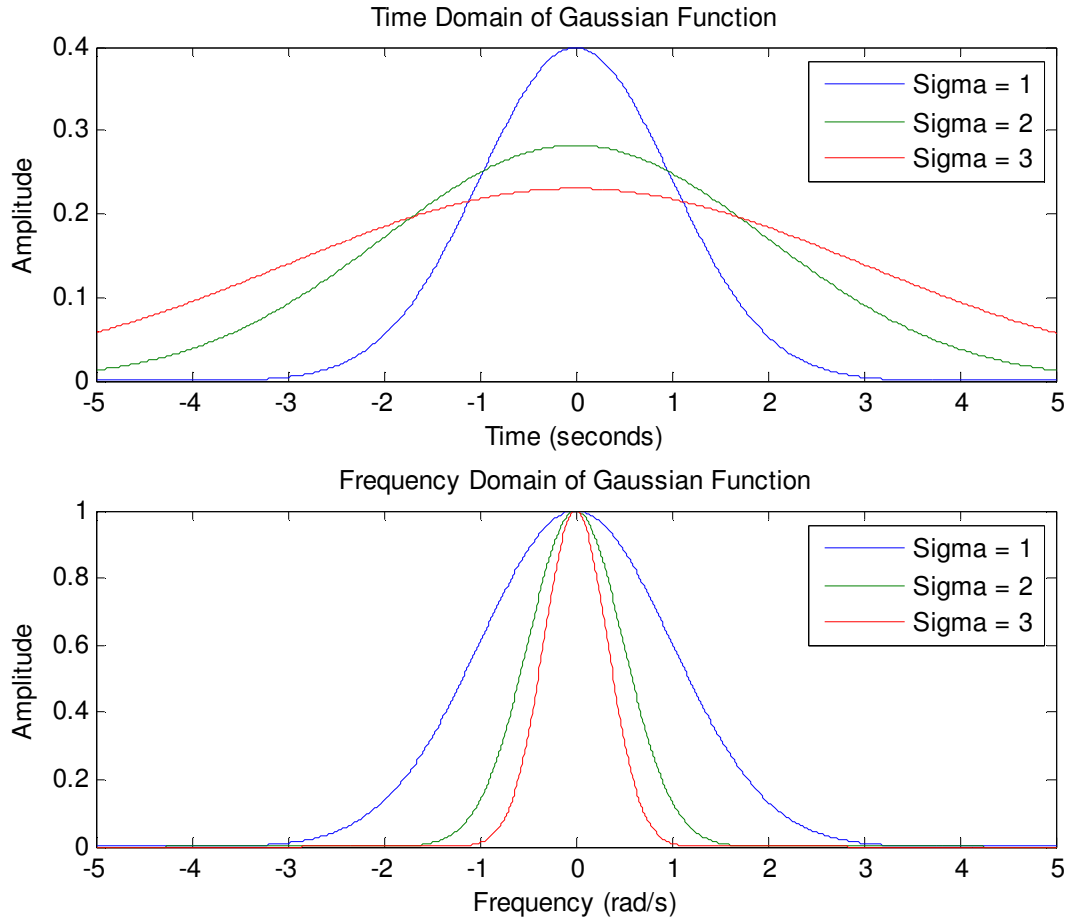


Figure 3.4 Time and Frequency Domain of Gaussian Function

Using the Gaussian pulse signal as an excitation of the nonlinear resonator, the bandwidth of the system can be determined by finding the input impedance via Discrete Fourier Transform.

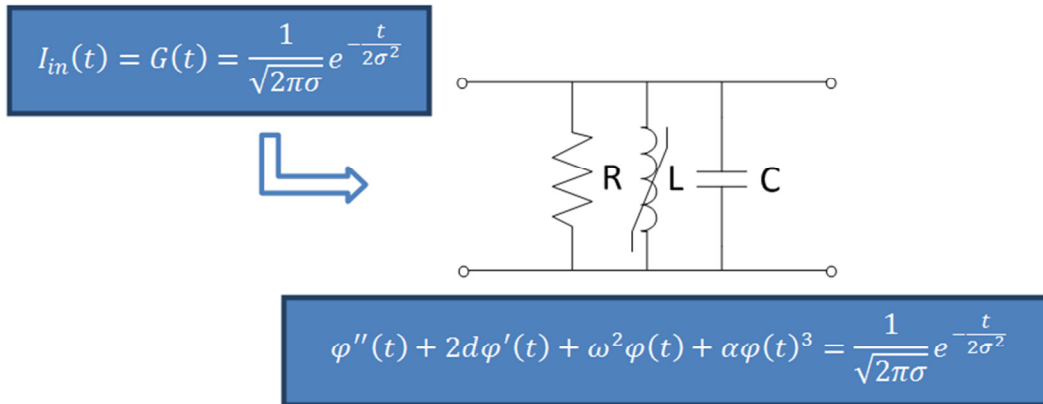


Figure 3.5 Nonlinear Resonator with its Differential Equation

The input impedance frequency response $Z_{IN}(\omega)$ can be calculated by computing the time domain input impedance and finding its Fourier transform. The frequency domain impedance is defined as

$$Z_{IN}(\omega) = \frac{V_{IN}(\omega)}{I_{IN}(\omega)} \quad (3.24)$$

Figure 3.6 shows the process used in computing the input impedance frequency response curves.

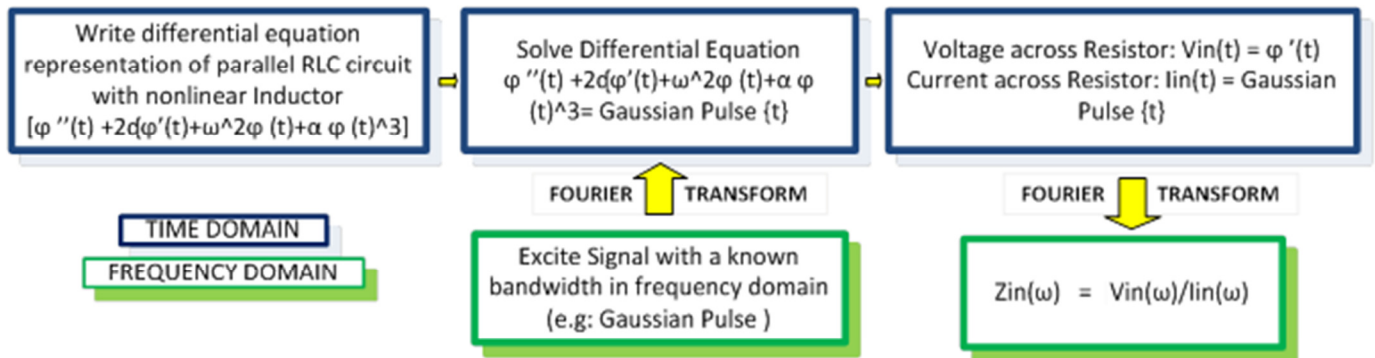


Figure 3.6 Nonlinear RLC Input Impedance Methodology

3.5 Numerical Simulation Results

In this section, numerical simulations are presented to show the input impedance of the narrowband nonlinear antenna model (Nonlinear Resonator). The numerical simulations are carried out using the methodology described in Figure 3.6 for three different cases. The plots compare a linear resonator ($\alpha = 0$) with one of nonlinearity. In the first case, the nonlinear coefficient α is varied for bandwidth improvement. In Case II, the excitation bandwidth is varied to examine any coloration between the nonlinearity the signal bandwidth. Finally in Case III, the excitation amplitude is increased and the nonlinear coefficient α is varied.

3.5.1 Case I: Variation in Nonlinear Factor

In this case, the nonlinearity in the parallel RLC circuit is varied only while keeping the excitation of the input signal constant. The equation describing the narrowband nonlinear antenna model is given by

$$\varphi''(t) + 2d\varphi'(t) + \omega^2\varphi(t) + \alpha\varphi(t)^3 = F \frac{1}{\sqrt{2\pi\sigma}} e^{-\frac{t}{2\sigma^2}} \quad (3.25)$$

where the values for the nonlinear resonator is given in Table 3.1. For all cases, the input impedance is normalized meaning the antenna is matched. The results show that the nonlinearity in a narrowband antenna does increase the bandwidth. For example, when the nonlinear coefficient is $\alpha = 0.12$, the bandwidth is doubled compared to a linear resonator. A summary of the results comparing the signal bandwidth is presented in Table 3.2.

Table 3.1 Parameters used to simulate nonlinear resonator modeled in Eq. (3.25)

Parameter	Selected Value
F	1
d	1
ω_o	1 rad/s
σ	100
α	varied

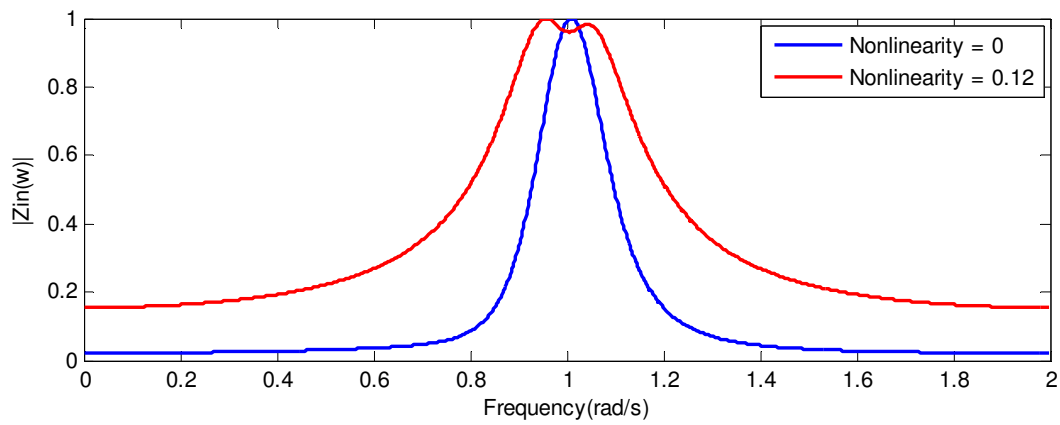


Figure 3.7 Comparison of Input impedance magnitude response for a system modeled in Eq(3.25) with nonlinearity ($\alpha = 0.12$). Other parameters defined in Table 3.1

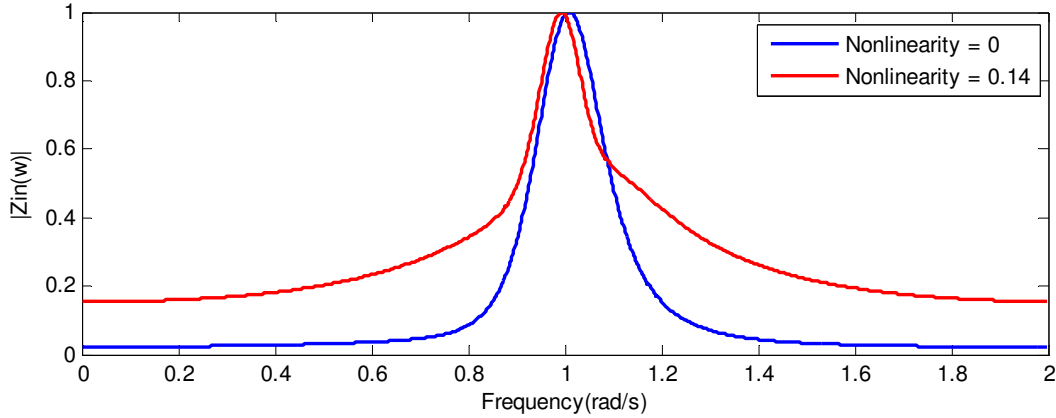


Figure 3.8 Comparison of Input impedance magnitude response for a system modeled in Eq(3.25) with nonlinearity ($\alpha = 0.14$). Other parameters defined in Table 3.1

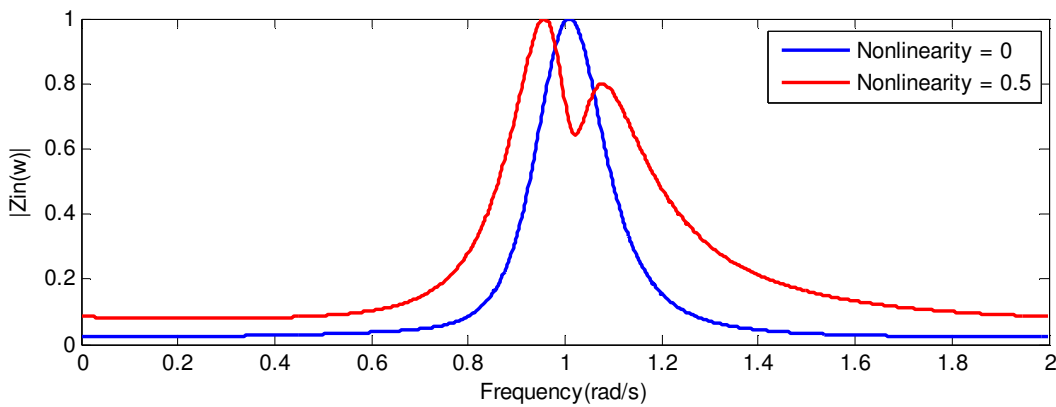


Figure 3.9 Comparison of Input impedance magnitude response for a system modeled in Eq(3.25) with nonlinearity ($\alpha = 0.5$). Other parameters defined in Table 3.1

Table 3.2 Input Impedance Bandwidth of RLC circuit with various nonlinear factors

Nonlinearity (α)	Input Signal Bandwidth ($\sigma = 100$)	Output Signal Bandwidth (rad/s)
$\alpha = 0$	$\sigma = 100$	0.12
$\alpha = 0.12$	$\sigma = 100$	0.27
$\alpha = 0.14$	$\sigma = 100$	0.11
$\alpha = 0.5$	$\sigma = 100$	0.23
* Results are Normalized in all cases (RLC circuit/Antenna Matched)		

3.5.2 Case II: Excitation Bandwidth and Nonlinearity Factor Varied

For this case, the excitation bandwidth increased and the nonlinearity in the circuit was varied.

Table 3.3 shows the rest of the parameters used in the simulation. Results show a bandwidth improvement, but there are cases in which the bandwidth doesn't change as shown in Figure 3.10. A summary of the results for this case is present in Table 3.4

Table 3.3 Parameters used to simulate nonlinear resonator modeled in Eq. (3.25)

Parameter	Selected Value
F	1
d	1
ω_o	1 rad/s
σ	120
α	varied

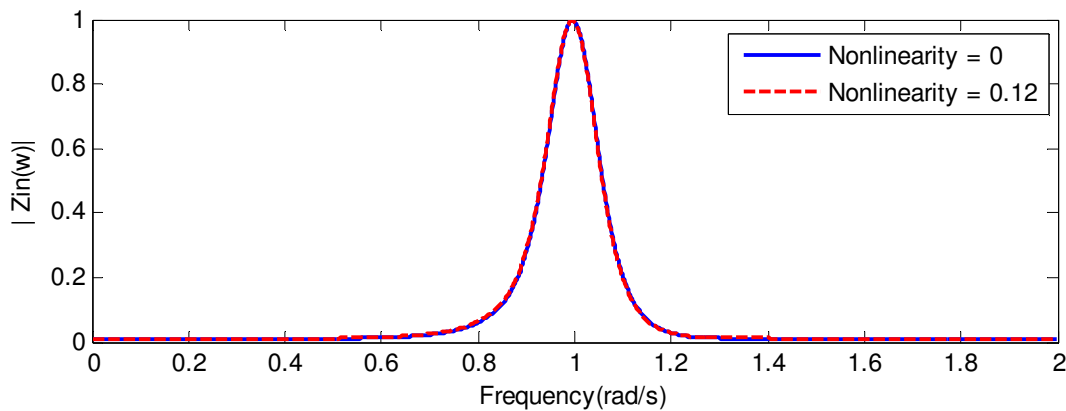


Figure 3.10 Comparison of Input impedance magnitude response for a system modeled in Eq (3.25) with nonlinearity ($\alpha = 0.12$). Other parameters defined in Table 3.3.

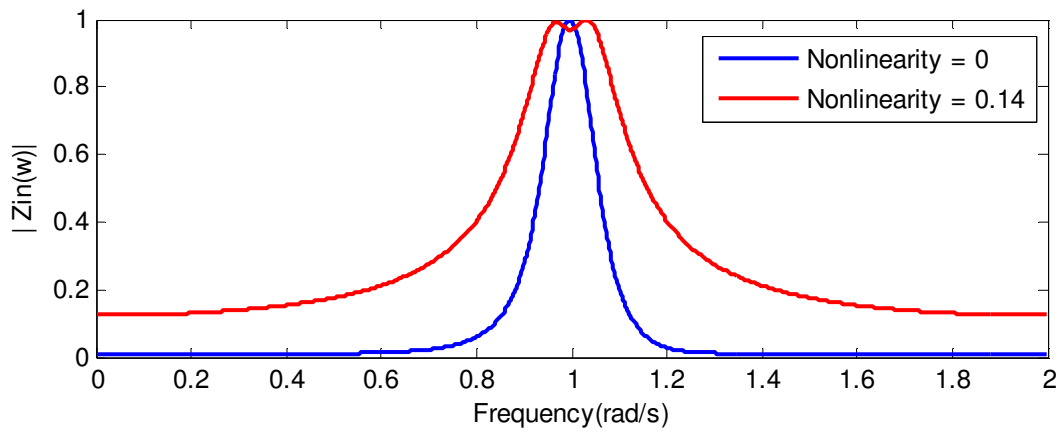


Figure 3.11 Comparison of Input impedance magnitude response for a system modeled in Eq (3.25) with nonlinearity ($\alpha = 0.14$). Other parameters defined in Table 3.3.

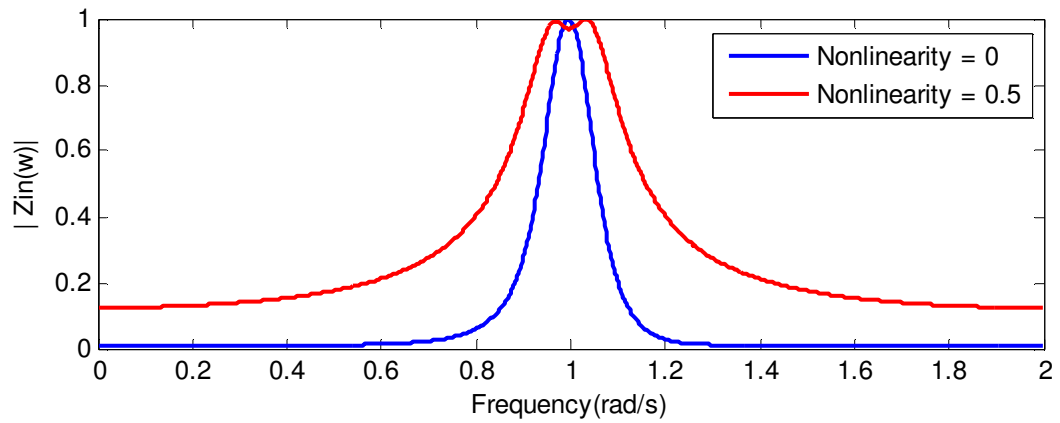


Figure 3.12 Comparison of Input impedance magnitude response for a system modeled in Eq(3.25) with nonlinearity ($\alpha = 0.5$). Other parameters defined in Table 3.3.

Table 3.4 Input Impedance Bandwidth of RLC circuit with various nonlinear factors

Nonlinearity (α)	Input Signal Bandwidth ($\sigma = 100$)	Output Signal Bandwidth (rad/s)
$\alpha = 0$	$\sigma = 120$	0.09
$\alpha = 0.12$	$\sigma = 120$	0.09
$\alpha = 0.14$	$\sigma = 120$	0.20
$\alpha = 0.5$	$\sigma = 120$	0.21
* Results are Normalized in all cases (RLC circuit/Antenna Matched)		

3.5.3 Case III: Excitation Amplitude and Nonlinearity Factor Varied

For this case, the excitation amplitude is increased and the nonlinearity in the circuit was varied.

Table 3.5 shows the rest of the parameters used in the simulation. Results show that strong nonlinearities contribute to a higher bandwidth improvement.

Table 3.5 Parameters used to simulate nonlinear resonator modeled in Eq. (3.25)

Parameter	Selected Value
F	5
d	1
ω_o	1 rad/s
σ	120
α	varied

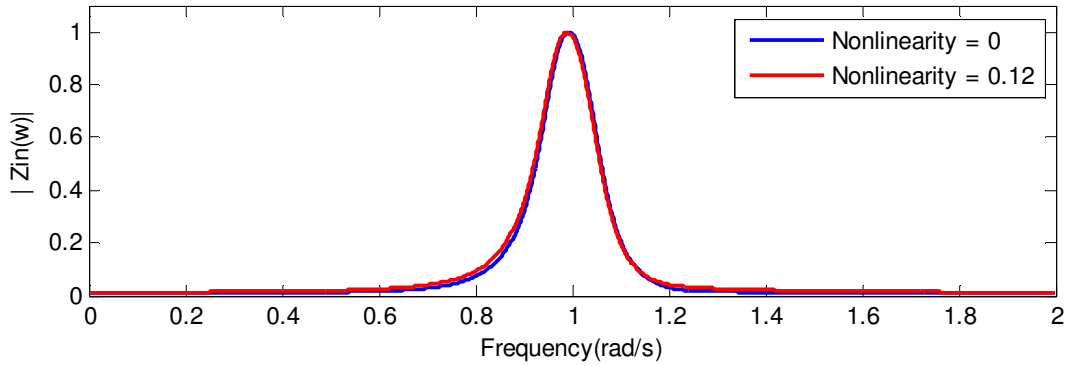


Figure 3.13 Comparison of Input impedance magnitude response for a system modeled in Eq with nonlinearity ($\alpha = 0.12$). Other parameters defined in Table 3.5.

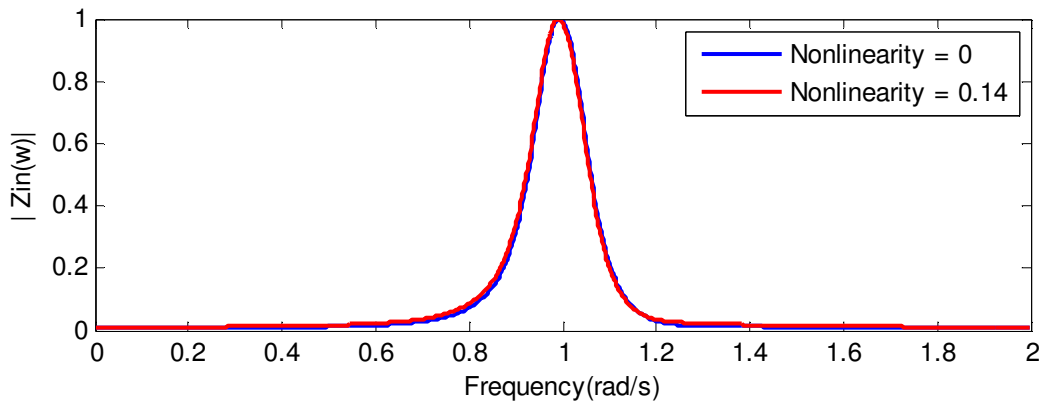


Figure 3.14 Comparison of Input impedance magnitude response for a system modeled in Eq with nonlinearity ($\alpha = 0.14$). Other parameters defined in Table 3.5.

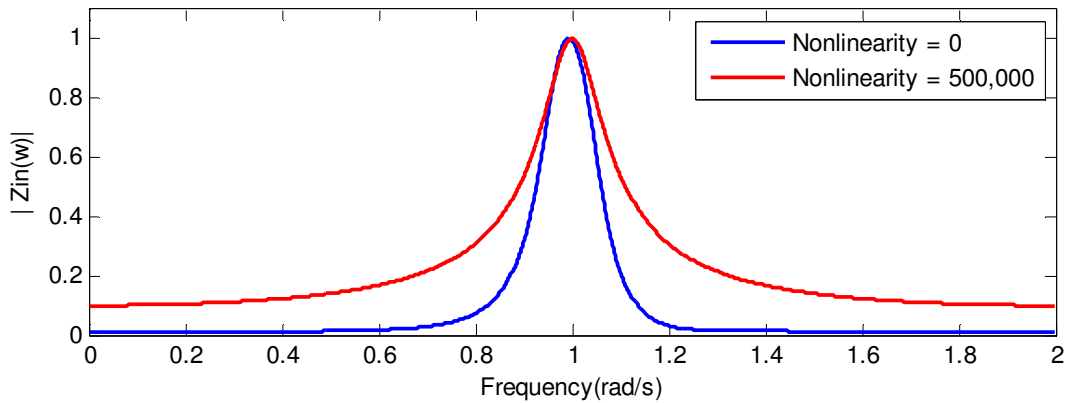


Figure 3.15 Comparison of Input impedance magnitude response for a system modeled in Eq with nonlinearity ($\alpha = 500,000$). Other parameters defined in Table 3.5.

Table 3.6 Input Impedance Bandwidth of RLC circuit with various nonlinear factors

Nonlinearity (α)	Input Signal Bandwidth ($\sigma = 100$)	Output Signal Bandwidth (rad/s)
$\alpha = 0$	$\sigma = 120$	0.09
$\alpha = 0.12$	$\sigma = 120$	0.10
$\alpha = 0.14$	$\sigma = 120$	0.10
$\alpha = 500,000$	$\sigma = 120$	0.124
* Results are Normalized in all cases (RLC circuit/Antenna Matched)		

References

- [1] David A. Sanchez-Hernandez, “Fundamental Antenna Properties Definitions” in *Multiband integrated antennas for 4G terminals*, 1st Edition, Spain: Artech House, Aug 2008
- [2] M.Pakdemirli, M.M.F. Karaham and H.Boyaci., “A New Perturbation Algorithm with Better Convergence Properties: Multiple Scales Lindstedt Poincare Method,” *Mathematical and Computational Applications*, Vol. 14, No.1, pp 31-44, 2009
- [3] W.Press, S.Teukolsky,W.Vetterling and B.Flannery. Numerical Recipes in FORTRAN 77. The Art of Scientific Computing. 2nd Edition, Cambridge University Press, 1992

Chapter 4 Low Profile Antennas for Wireless Communications

In the previous chapter, a narrowband nonlinear loaded antenna was modeled as a nonlinear RLC circuit with a nonlinear inductor acting as the ferromagnetic material. Based on the numerical results, there was an increase in the input impedance bandwidth. This chapter presents a look at various low profile antenna design structures in which ferromagnetic material loading is possible. Section 4.1 starts with an introduction and analysis of the Inverted-L Antenna. Section 4.2 and Section 4.3 presents the Inverted-F Antenna and Planar Inverted-F Antenna respectively.

4.1 The Inverted-L Antenna

The Inverted-L Antenna is basically a monopole antenna folded down with part of the antenna parallel to the ground plane as shown in Figure 4.1. It is used in applications where a low profile antenna is needed and a narrow bandwidth is acceptable [1]. The monopole is bent parallel to the ground plane after some distance to save space. The tradeoff for saving space is a decrease in the radiation resistance due the part of the antenna being parallel with the the ground plane.

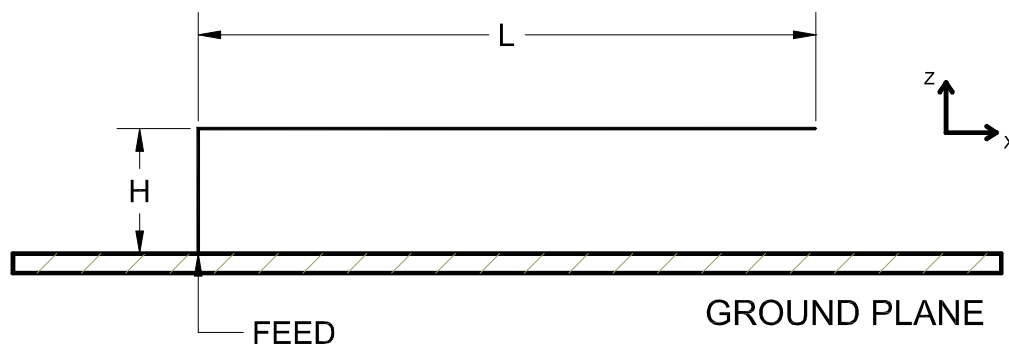


Figure 4.1 The Inverted-L Antenna geometry

4.1.1 Frequency Analysis and Radiation Pattern

The total length of the antenna including the vertical and horizontal length sums up to a quarter of a wavelength. The antenna therefore resonates when

$$\frac{\lambda}{4} \approx (L + H) \quad (4.1)$$

The height, h of the antenna is very small compared to the wavelength. Like a traditional monopole antenna, the current distribution of the Inverted-L is sinusoidal over the length of the wire with its maximum current at the midpoint of the wire and its minimum at the endpoint. It is also important to note the current contributing to the vertical portion of the wire can be neglected

because the height is small compared to the wavelength and the horizontal currents are nearly out of phase in the far field [1].

The radiation pattern of the ILA resembles that of a monopole antenna except there is additional E_θ due to the horizontal length of the antenna. There is also a slight distinction from the monopole in that is a dip rather than a perfect null at the z- axis [1]. Nevertheless, the ILA provides omni-directional far-field coverage in azimuth.

4.1.2 Input Impedance

One of the disadvantages of using the ILA for low profile applications is its unattractive input impedance. Because a large section of the antenna is bent parallel to the ground plane, the open circuit adds a large capacitance to the input impedance. As a result the impedance has a low resistance and it highly reactive [2]. Therefore an additional matching network needs to be added to match the input impedance to the typical 50 ohms. Equations 4.2 and 4.3 show the approximations of the input impedance [3]

$$R_r = 160\pi^2 \left(\frac{h}{\lambda}\right)^2 \left[1 - \frac{h}{2(h + L_H)}\right]^2 \quad (4.2)$$

$$X_L = \frac{-60h \left(2 - \frac{h}{h + L_H}\right)}{k(h + L_H)^2} \left[\begin{aligned} & \ln\left(\frac{2h}{a}\right) - \frac{a}{h} + \frac{L_a T - h}{\sqrt{L_a^2 + h^2}} - \frac{5(kh)^2}{8} \\ & + \left\{ \frac{k^2 h^2}{2} \left(1 + \frac{L_H}{h}\right)^2 \right\} \ln\left(\frac{2h}{a}\right) \\ & + \frac{k^2 h^2}{2} \sqrt{1 + \frac{L_a^2}{h^2}} + \frac{k^2 h^2}{2} T \ln\left(\frac{L_a + \sqrt{L_a^2 + h^2}}{h + a}\right) \end{aligned} \right] \quad (4.3)$$

Where k is the wave number ($2\pi/\lambda$), h is the antenna height, L is the antenna length, a is the wire radius, $L_a = L_H + a$ and $T = 1 - a/h$. Although the ILA is a fairly simple structure to

design and integrate into low profile applications, it comes at a prize of adding an additional matching network to because of its input impedance. The best solution is to modify the ILA by adding another segment to form the Inverted - F Antenna.

4.2 The Inverted-F Antenna



Figure 4.2 The Inverted- F Antenna

The Inverted-F Antenna (IFA) is a slight modification of the Inverted-L Antenna. It can be viewed as two Inverted-L combined together forming an inverted F as seen in Figure 4.2. Like the Inverted-F Antenna, is it also a quarter wave vertical antenna bent horizontally (parallel to the ground plane). The major difference between the Inverted-F antenna and the Inverted-L Antenna is that the latter has another element short circuited to the ground plane. This allows the input impedance to be fairly managed and can be optimized by changing the distance from the fed to the short circuit element [1].

4.2.1 Frequency Analysis and Input Impedance

The IFA resonates when

$$\frac{\lambda}{4} \approx (L + H) \quad (4.4)$$

The distance s between the short circuit element and the feed can be changed to increase or decrease the inductance of the circuit. The idea here is to change manage to the distance such that the inductance to the left cancels the capacitance to the right, leaving just the radiation resistance [5]. The feed location plays an important role in the radiation resistance of the IFA—for instance, if the antenna is fed at the center (maximum voltage and minimum current), the radiation resistance will be high and the antenna wouldn't radiate. With this analysis, an equivalent parallel RLC lumped circuit can be used to represent the IFA.

Another important design constrain of the IFA is its height and length of the ground plane. The height of the ground plane should be at least a quarter wavelength and the length should be as wide as the IFA length L [5]. The radiation pattern becomes increasing multi-lobed if the ground plane is much longer than the IFA length. In contrast, if the ground plane is smaller than the IFA length, tuning becomes increasingly difficult and the overall performance degrades [6]. In terms of radiation pattern, the IFA is similar to the ILA in that it has a donut shape with “dips” on the z-axis.

While the IFA is an upgrade over the ILA, it still has its limitations. The bandwidth is typically 2% around the center frequency for cellular applications. To enhance the bandwidth of the IFA, the top section is replaced by metallic planes forming the Planar Inverted-F Antenna (PIFA).

4.3 The Planar Inverted-F Antenna

The Planar Inverted-F Antenna (PIFA) is a variation from the simple Inverted F (IFA) Antenna. PIFAs are quickly becoming popular in mobile communication systems due to their small size, simple impedance match and the ability to provide both vertically and horizontally polarized

electric fields [4]. Another advantage of the PIFA is that it has a wider bandwidth compared to the ILA and IFA; a typical PIFA can achieve about 8% bandwidth in most cellular applications compared to the about 1 - 2% with the ILA or IFA. Secondly, the PIFA is designed in a way that reduces the backward radiation towards the user's head [6].

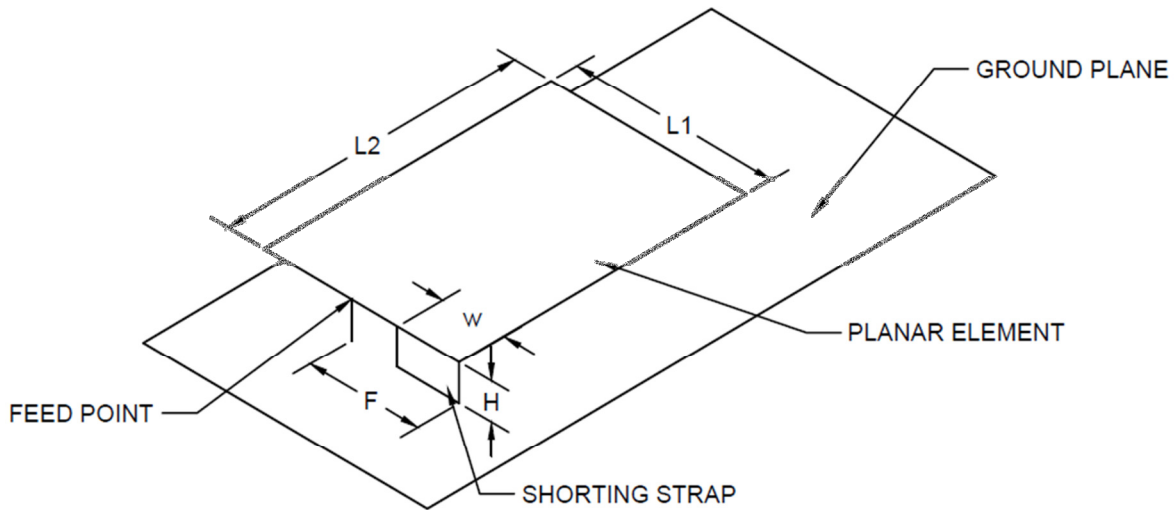


Figure 4.3 The Planar Inverted-F Antenna

4.3.1 Frequency Analysis

Figure 3.3 shows the dimensions of a typical Planar Inverted-F Antenna. It is similar to the conventional patch antenna in that it is on top of a dielectric with permittivity; therefore the wavelength is calculated using Equation (4.5)

$$\lambda = \frac{c}{f\sqrt{\epsilon_r}} \quad (4.5)$$

The top plate has two dimensions, the length L1 and the width L2, raised at a height h, above the ground plane. There is a shorting plate of width W on the edge of top plate which has an effect on the resonant frequency. Lastly the PIFA is fed at a distance F away from the shorting plate.

When the feed point is closer to the shorting plate, the impedance decreases and when the feed point is move further from the edge, the impedance increases [7]. The resonant frequency of the PIFA depends on the length, width, height and shorting plate as shown in Equation (4.6)

$$\frac{\lambda}{4} = L1 + L2 + H - W \quad (4.6)$$

Typically, the height h , is really small compared the wavelength so it can be neglected. When the shorting plate covers the entire width of the plate ($W = L2$), the antenna will radiate when

$$\frac{\lambda}{4} = L1 + H \quad (4.7)$$

And when the width of the shorting plate is zero, the antenna will radiate according to Equation (3.8).

$$\frac{\lambda}{4} = L1 + L2 + H \quad (4.8)$$

Furthermore, increasing the width of the shorting plate not only impacts the resonant frequency but also the surface current on top of the plate and the impedance bandwidth.

4.3.2 Bandwidth of Planar Inverted-F Antenna

The bandwidth of the PIFA is dependent on a variety of factors. Because the PIFA is loaded on top of a substrate, the bandwidth increases when the dielectric constant is small. This is due to the fact that substrates with high dielectric constant tend to store energy more than radiate it. In the same way, increasing the substrate height decreases the energy stored in the PIFA, plus leading to a higher bandwidth [6].

Another important factor that affects the bandwidth of the PIFA is the shorting plate width. PIFAs tend to have the highest bandwidth when the shorting plate covers the whole width.

On the other hand, when the shorting plate width reduces in size, the bandwidth tends to decrease dramatically [8]. The height of the PIFA is the most critical parameter in controlling the bandwidth; increasing the height can triple the -10dB bandwidth of a single band PIFA [9]. However there is a limit in how high the height of the PIFA can be depending on the design of the wireless device.

References

- [1] W.L Stutzman and G.A. Thiele, *Antenna Theory and Design*, New York: John Wiley & Sons, Inc., 1998
- [2] J. P Abelairas and F. M Martin, "Techniques to reduce the Mutual Coupling and improve the Isolation between antennas in a Diversity System," Project Report, Aalborg University, January 2010.
- [3] A. Gobien. "Investigation of low profile antenna designs for use in hand-held radios," Master's thesis, Virginia Polytechnic Institute and State University, August 1997
- [4] Fujimoto, K., Henderson, A., Hirasawa, K., James, J.R. *Small Antennas*, Research Studies Press Ltd., London and John Wiley & Sons Inc., New York, 1987.
- [5] Bevelacqua, P. "The Inverted-F Antenna." Internet: <http://www.antenna-theory.com/antennas/aperture/ifa.php>, [Dec.2, 2011].
- [6] I.Rosu, "PIFA-Planar Inverted F Antenna," Internet: http://www.qsl.net/va3iul/Antenna/PIFA/PIFA_Planar_Inverted_F_Antenna.pdf, Nov. 11, 2001 [Dec. 2, 2011].
- [7] Bevelacqua, P. "The Inverted-F Antenna." Internet: <http://www.antenna-theory.com/antennas/patches/pifa.php>, [Dec.2, 2011].
- [8] N. P. Cummings. "Low Profile Integrated GPS and Cellular Antenna," Master's thesis, Virginia Polytechnic Institute and State University, Blacksburg, VA 24060, October 2001
- [9] Z. Zhang, *Antenna Design for Mobile Devices*. Singapore: John Wiley & Sons (Asia) Pte Ltd., 2011

Chapter 5 Down selection of Low Profile

Antenna

This chapter presents a design and simulation of a narrowband low-profile antenna. Based on analysis discussed in Chapter 4, the Planar-Inverted μ -F Antenna (PIFA) is the best candidate because of its variety to control and tune the antenna. Section 5.1 presents the structure design and simulation results for the narrowband antenna. Next, a modification of the antenna structure is discussed for nonlinear loading. Section 5.2 describes the design process and simulation results for a nonlinear Planar Inverted- F Antenna for bandwidth improvement.

5.1 Linear PIFA Antenna

For this section, a planar inverted – F antenna is designed to resonate around 1 GHz. The dimensions are described in Table 5.1 and detailed in Figure 5.1. The antenna structure has a top radiating plate that is 40 mm long and 28 mm wide located 5mm above the ground plane. The dimensions of the ground plane are 120mm by 84 mm. The feed pin is a coaxial probe that is located a distance 25.8mm from the right end of the radiating plate. The shorting plate is 1mm wide and is a location at the lower right end of the radiating plate.

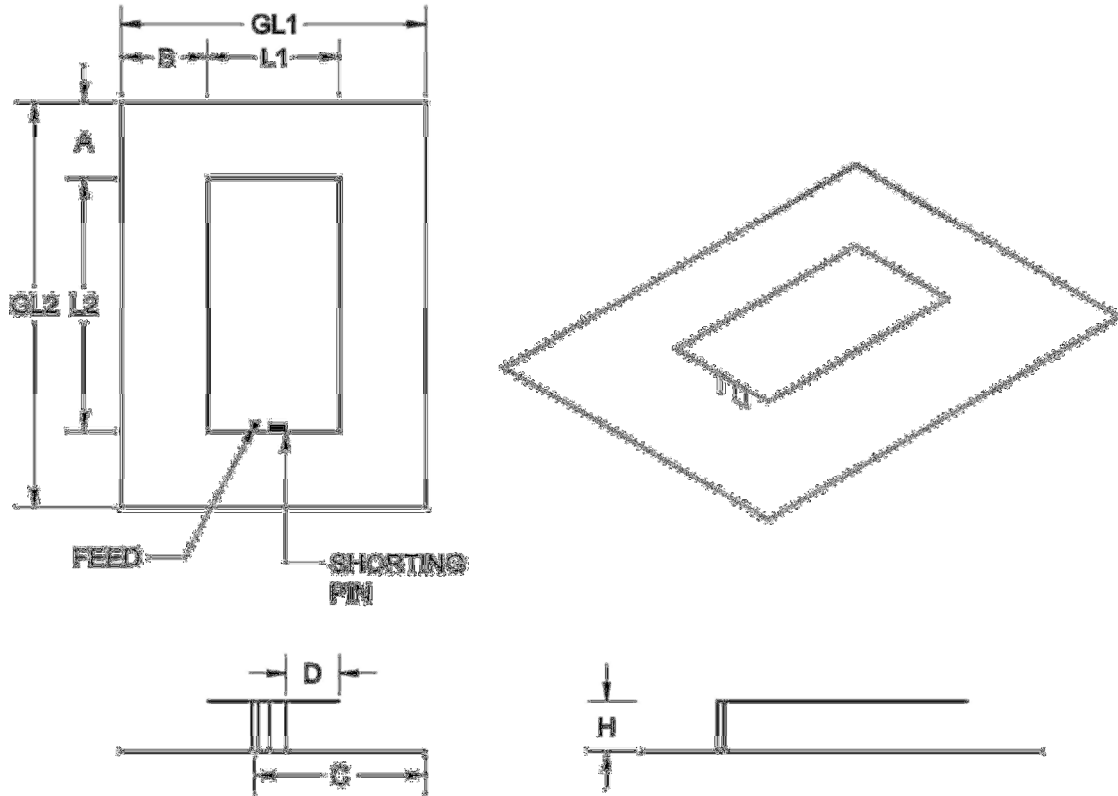


Figure 5.1 Planar Inverted-F Antenna (1 GHz)

Table 5.1 Dimensions for 1 GHz PIFA: Geometry layout is shown in Figure 5.1

ANTENNA DIMENSIONS (mm)		
L1 = 28	L2 = 40	A = 40
B = 28	H = 5	GL1 = 84
GL2 = 120	D = 25.8	C = 27

5.2 Simulated Results

This section presents the simulated results for the antenna dimensions in Table 5.1. The reflection coefficient is shown in Figure 5.2 and the input impedance is Figure 5.3. The real part of the input impedance has maximum of 250 ohms at 1 GHz. The imaginary part of the impedance is 0 at 1 GHz. The reflection coefficient suffers because the input impedance isn't close the matched 50 ohm load.

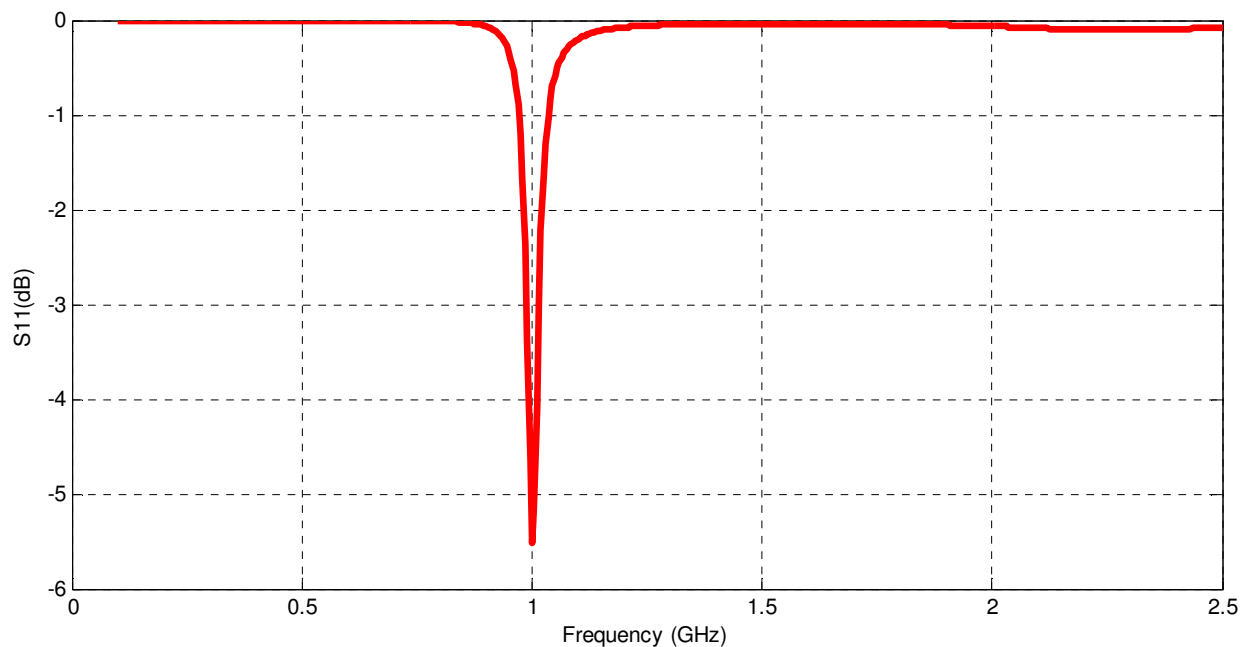


Figure 5.2 Reflection Coefficient versus frequency of planar inverted-F antenna

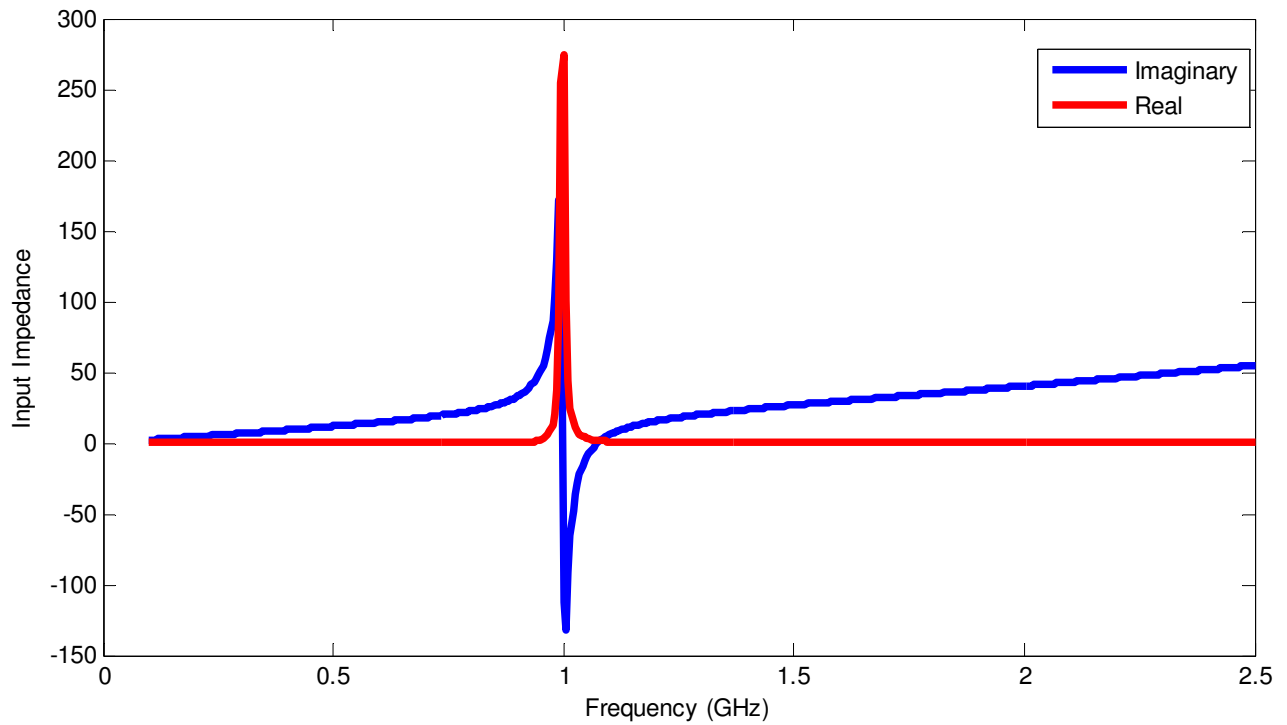


Figure 5.3 Input Impedance versus frequency of planar inverted-F antenna

5.2.1 Far-Field Radiation Pattern

Figure 5.4 shows the radiation pattern calculation in 3D. 2D cuts of the radiation pattern $E_{\theta}(\varphi = 0^{\circ})$ and $E_{\theta}(\varphi = 90^{\circ})$ are shown in Figure 5.5. The azimuth $E_{\theta}(\theta = 90^{\circ})$ and $E_{\varphi}(\theta = 0^{\circ})$ are shown in Figure 5.6.

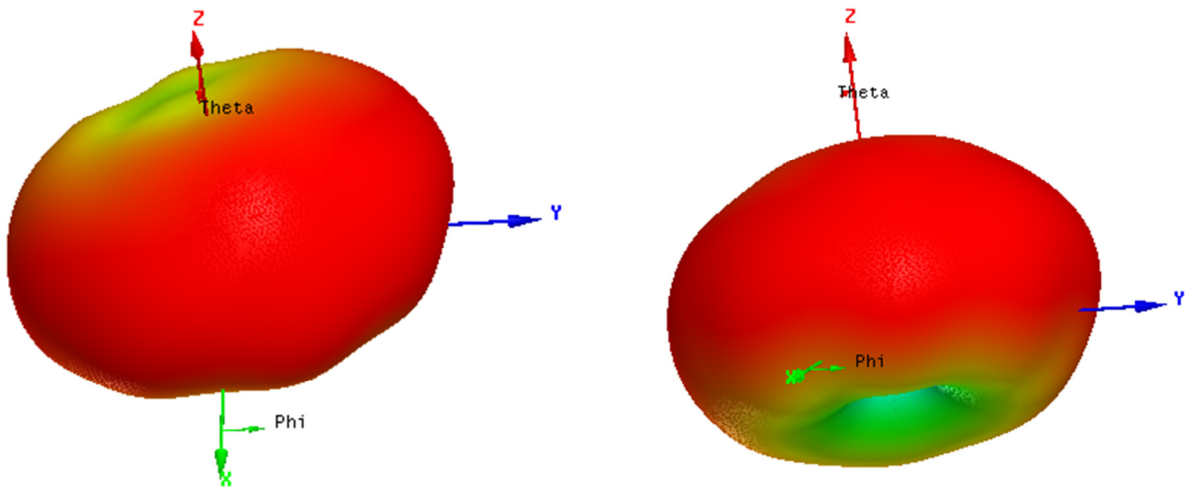


Figure 5.4 3D Total Radiation Pattern of PIFA

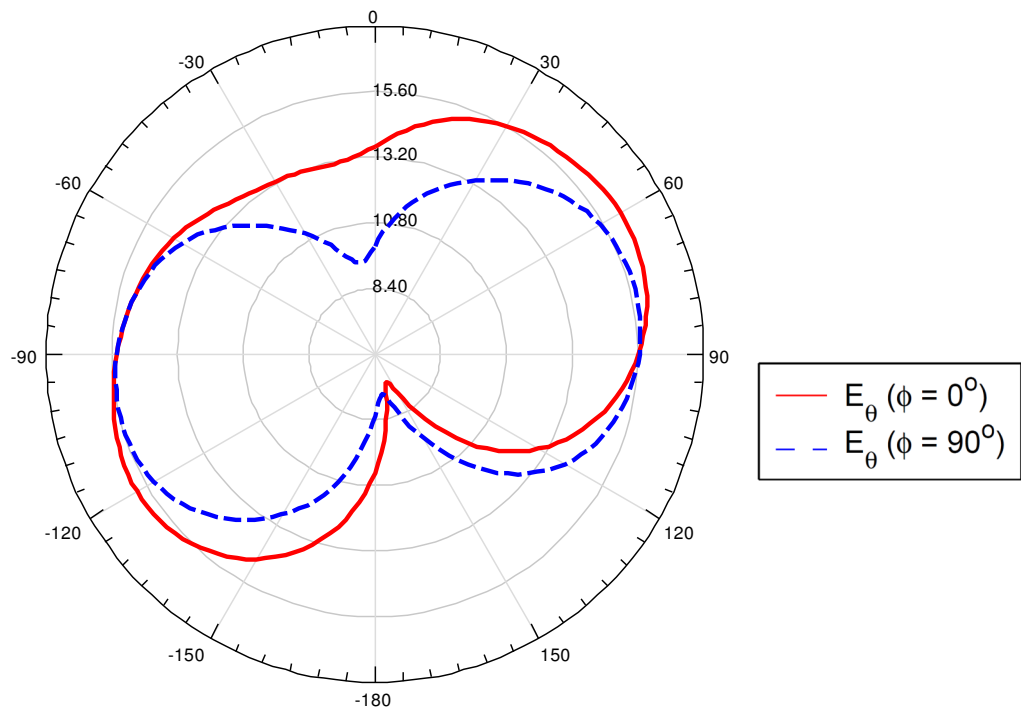


Figure 5.5 Calculated Radiation Patterns, $E_{\theta}(\phi = 0^{\circ})$ and $E_{\theta}(\phi = 90^{\circ})$

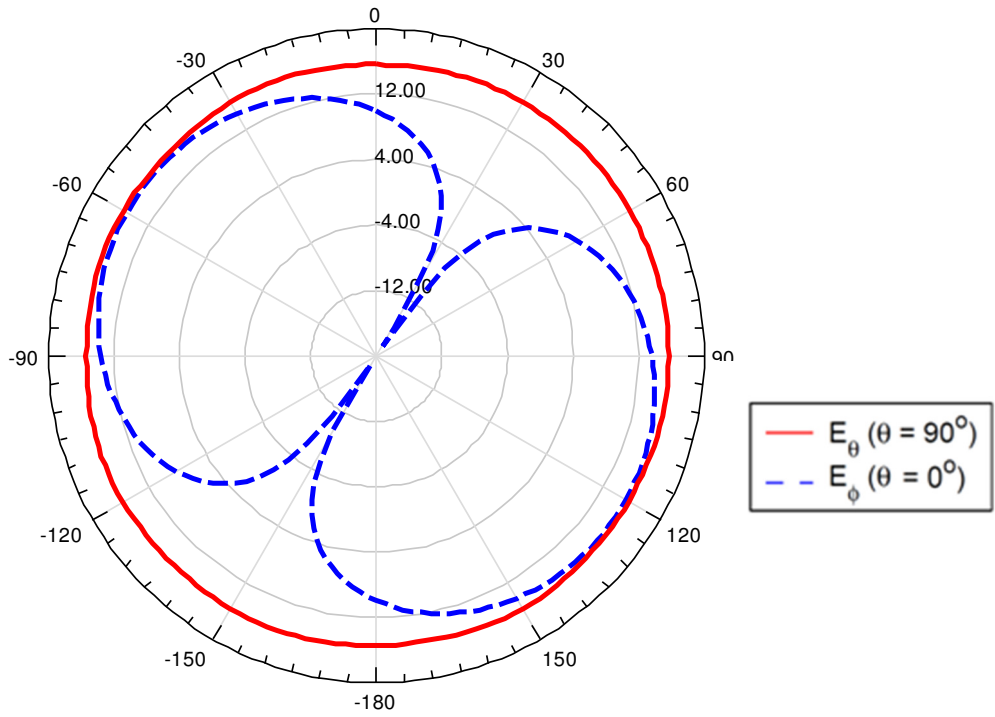


Figure 5.6 Calculated Radiation Patterns, $E_\theta(\theta = 90^\circ)$ and $E_\phi(\theta = 0^\circ)$

5.3 PIFA Structure Variation on Input Impedance and Bandwidth

It is important to note how antenna parameters affect the behavior of the structure in terms of input impedance matching and consequently the reflection coefficient. The design process and ultimately the optimization process become less tedious when one knows what parameters to change in the antenna. This section illustrates how variations in antenna height and the spacing between feeding pin and shorting pin change the input impedance and reflection coefficient.

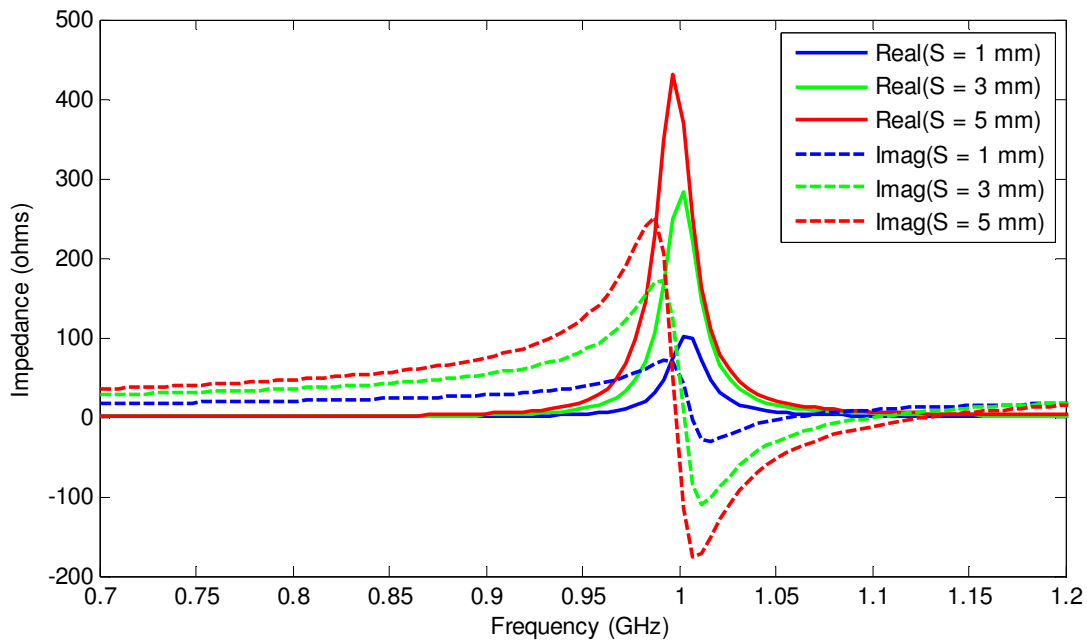


Figure 5.7 Input Impedance versus frequency for PIFA with various separation distance

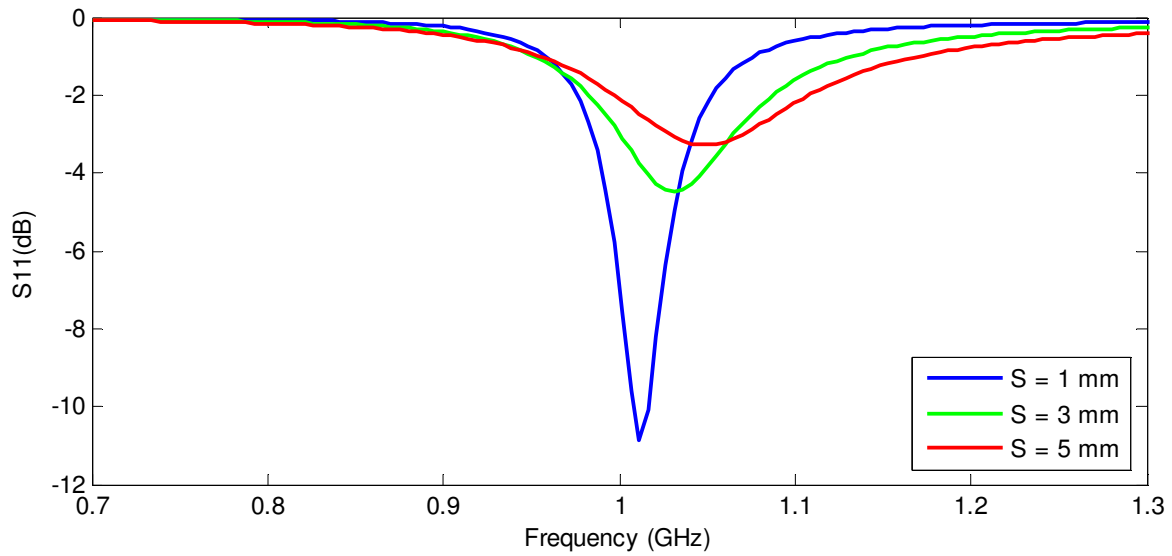


Figure 5.8 Impact of dimension S on reflection coefficient

Figure 5.7 illustrates the results when the distance between the feed point and the shorting pin is varied. As seen the figure, the real part of the input impedance increases when the separation distance is increased. Similarly, the imaginary part of the impedance is enlarged. Likewise, the reflection coefficient is affected. Since the antenna is matched to 50 ohms, the bandwidth suffers because of the impedance mismatch. Figure 5.8 shows that when separation distance is increased, the reflection efficient also suffers.

Figure 5.9 on the other hand shows the antenna response as its height is varied. When the antenna height is increased, the bandwidth increases as well. Contrarily, the resonant frequency reduces with an increase in height. Therefore, the height of the PIFA seems to be a critical factor because it controls both the resonant frequency and the bandwidth. However, because the goal is to miniaturize the antenna, the height is desired to be as low as possible.

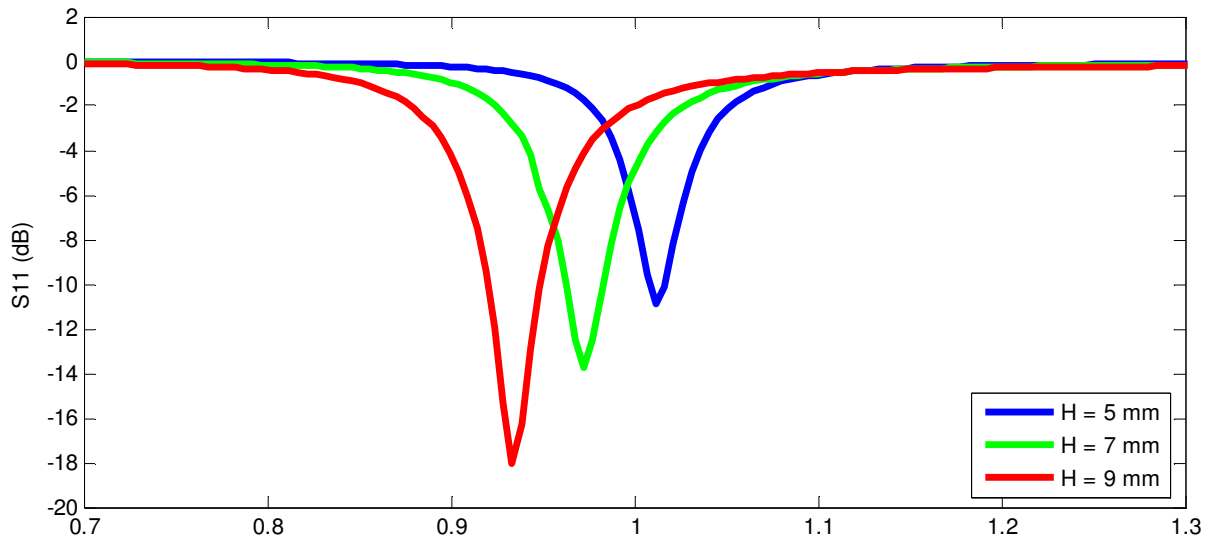


Figure 5.9 Impact of PIFA height on reflection coefficient

Chapter 6 A Nonlinear Tuned PIFA Antenna

This chapter presents design modifications on the Planar Inverted – F Antenna in order to load a nonlinear element. It also discusses the simulation setup used to effectively predict the behavior of the nonlinear antenna. Furthermore, it discusses the EM field simulator (HFSS) and RF electronic design automation software (ADS) used in cross-communication. The algorithm used to simulate the behavior of the nonlinear element is also discussed in the section. Simulation results of the nonlinear antenna are presented in section 6.3 and 6.4. Finally, section 6.5 discusses concerns regarding nonlinearity in the antenna structure.

6.1 Methodology and Algorithms

Typically, modeling a nonlinear device by itself is a huge task; one has to use or design a model that mimics its actual behavior. Combined with the task of predicting the response of an antenna loaded with a nonlinear device, extra care is needed to effectively simulate the response of the antenna. This section details the methodology and algorithms used in the antenna simulation.

6.1.1 Antenna Field Simulator and RF Simulator

The Electromagnetic (EM) field solver used in this thesis is HFSS. It is a finite element method based full EM analysis software used in antenna design and other complex RF structures. However, the full wave, frequency-domain simulation package doesn't utilize a nonlinear lumped element. Therefore, a methodology is needed to accurately simulate the behavior of the antenna with a nonlinear element. The methodology involves changing the antenna into a two port network and exporting the parameter data into an RF circuit simulator. The RF circuit simulator used is Advanced Design System (ADS) which is excellent for predicting the behavior of circuits with nonlinearities.

6.1.2 Exporting Scattering Parameters in ADS

Cross-communication between ADS and HFSS requires the use of importing scattering parameters from HFSS to ADS. HFSS calculates the two port scattering parameters matrix at the simulated sweep frequencies. The S-Parameters data is then imported to ADS for nonlinear analysis. In ADS, the first port is attached to an RF source and the second port to a nonlinear inductor. The reflection coefficient response is then calculated using the Large-Small Signal Parameters (LSSP) and Harmonic Balance (HB) algorithm. Figure 6.1 shows the circuit layout in ADS and Figure 6.2 shows a summary of the methodology used the nonlinear antenna design.

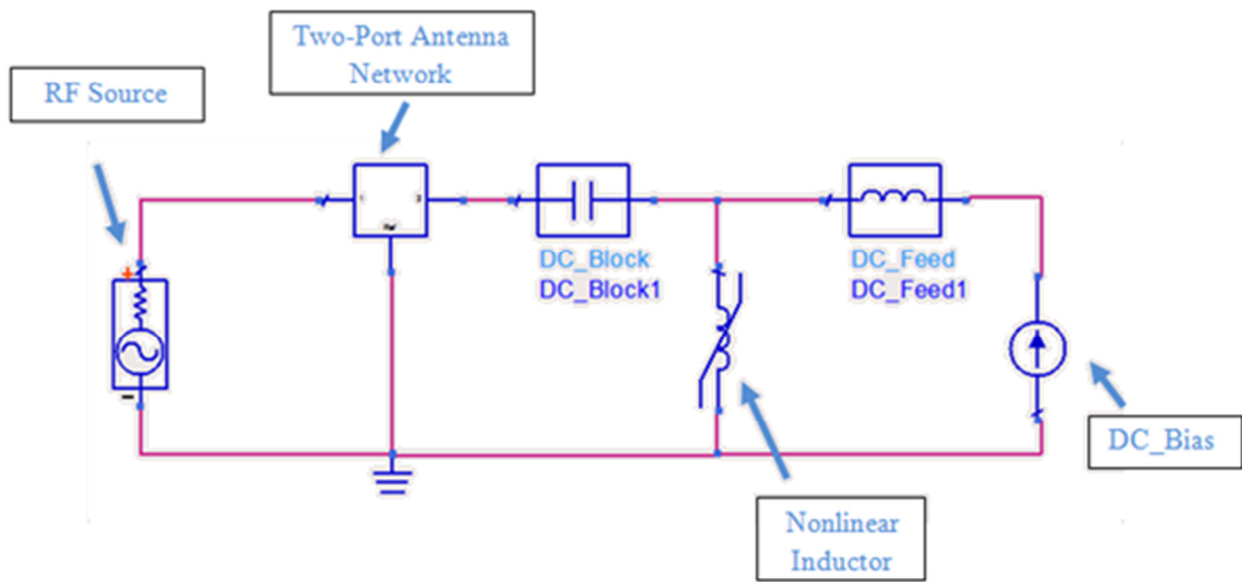


Figure 6.1 ADS Two-Port Antenna Simulation

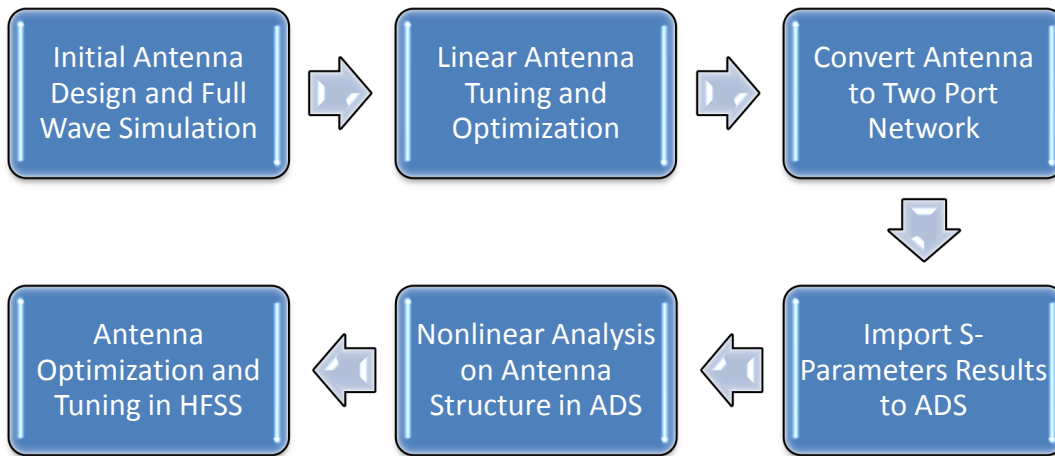


Figure 6.2 Methodology in Nonlinear Antenna Design

6.1.3 RF Algorithms: Harmonic Balance and LSSP Parameters

Harmonic Balance The classic “frequency response” simulation for linear circuits doesn’t work for a circuit with a nonlinear element. For this case, Harmonic Balance is used for the simulation. Harmonic Balance is basically a technique used to find the steady – state response of

a circuit containing any nonlinear components. First, the Harmonic Balance method works by separating the linear and nonlinear portion of the circuit. While linear circuit components are solely modeled in the frequency domain, the non-linear components are first modeled in time domain and Fourier-transformed before each solving step [1]. The goal of the Harmonic Balance algorithm is to make sure the sum of the linear and nonlinear currents at each node of the circuit is essentially zero.

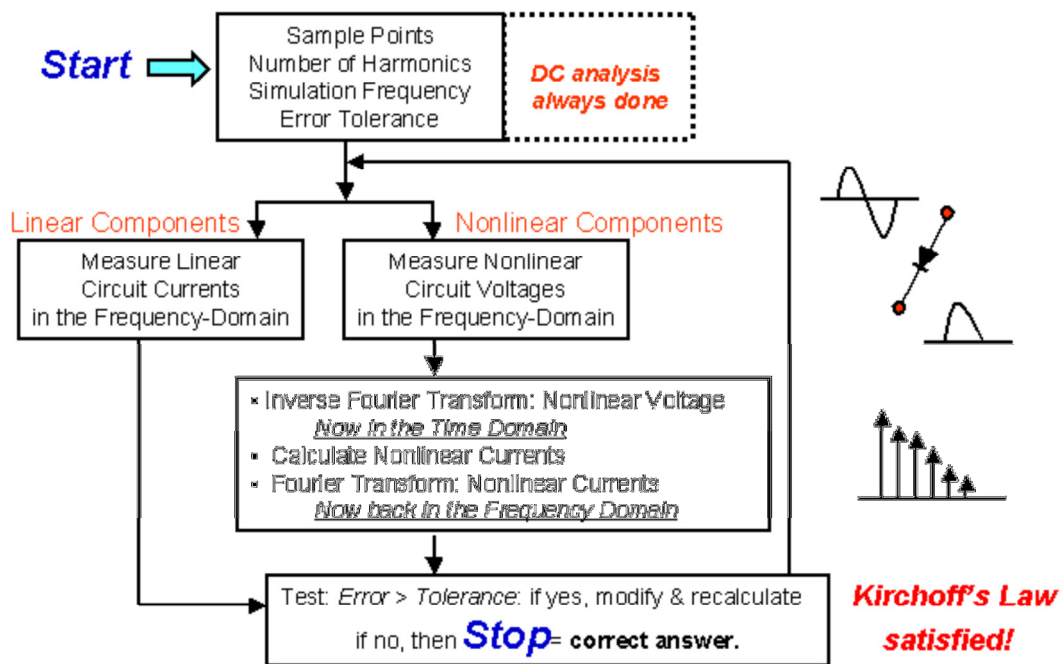


Figure 6.3 Harmonic Balance Simulation Steps

In addition, an error function of the circuit is calculated using circuit theory laws. For the nonlinear portion of the circuit, it's time domain voltages and currents are converted into respective harmonics and then included into the error function. If the error function calculated is larger than a threshold tolerance value, the analysis is modified and recalculated until the error function is less than the tolerance. Figure 6.3 shows a summary of the Harmonic Balance simulation steps.

Large-signal S-Parameter Large-signal S-Parameter (LSSP) is a method to compute S – parameters for circuits with nonlinear elements. LSSP simulation uses Harmonic Balance simulation to compute the S parameters of the nonlinear circuit, unlike small signal S-parameters that are computed on a small-signal simulation of the linearized circuit. Another major difference between S-parameters and Large-Signal S-Parameters is that LSSP are power-dependent. In other words, LSSP solutions can change as their power levels are varied [2].

In terms of mathematical definitions, Large-Signal S-parameters is defined as the ratio of reflected and incident waves as shown in Equation 1,

$$S_{ij} = \frac{B_i}{A_j} \quad (6.1)$$

where B_i and A_j are the reflected and incident waves respectively. The reflected and incident waves are defined as follows:

$$B_i = \frac{V_i - Z_{0i}^* I_i}{2\sqrt{R_{0i}}} \quad (6.2)$$

$$A_j = \frac{V_j + Z_{0j} I_j}{2\sqrt{R_{0j}}} \quad (6.3)$$

In Equations 2 and 3, Z_{0i} and Z_{0j} are reference impedances at their respective ports i and j. R_{0i} and R_{0j} are real parts of reference impedances Z_{0i} and Z_{0j} . V_i and V_j are Fourier coefficients voltages at the fundamental frequency at their ports. Similarly, I_i and I_j are Fourier coefficients currents at the fundamental frequency of ports i and j.

6.2 Nonlinear Antenna Structure

In chapters 2 and 3, it was noted that narrowband antennas behave like parallel RLC resonators around its resonant frequency. Therefore loading an inductive element to the antenna will cause a shift in the resonant frequency. This illustration is similar to attaching a shunt inductor to a parallel RLC resonator—the added inductance will change the total inductance of the circuit and shift its resonant frequency. With that in mind, the structure of the antenna is to be modified to compensate for the added element. The added benefit is that the PIFA can be miniaturized and then tuned with the nonlinear element. Table 6.1 shows the new dimensions of the modified PIFA structure.

Table 6.1 Nonlinear Antenna Dimensions

Parameter	Dimension (mm)
Length	20
Width	10
Height	5
Ground Plane Size	35 by 30

In practice, the nonlinear element should be attached from the ground plane to the radiating plate. To model this arrangement, the shorting pin is replaced with a second feeding pin. The second feeding pin essentially acts like another port where the nonlinear element would be placed. This configuration works best because the grounding strip functions as a shunt inductor. Since the nonlinear device loaded to the antenna is inductive, it acts as a lumped grounding strip. The optimal location to load the ferromagnetic material was close to the feed pin because current is the highest. Figure 6.4 shows the current density of the PIFA antenna which validates a high current at the feed pin.

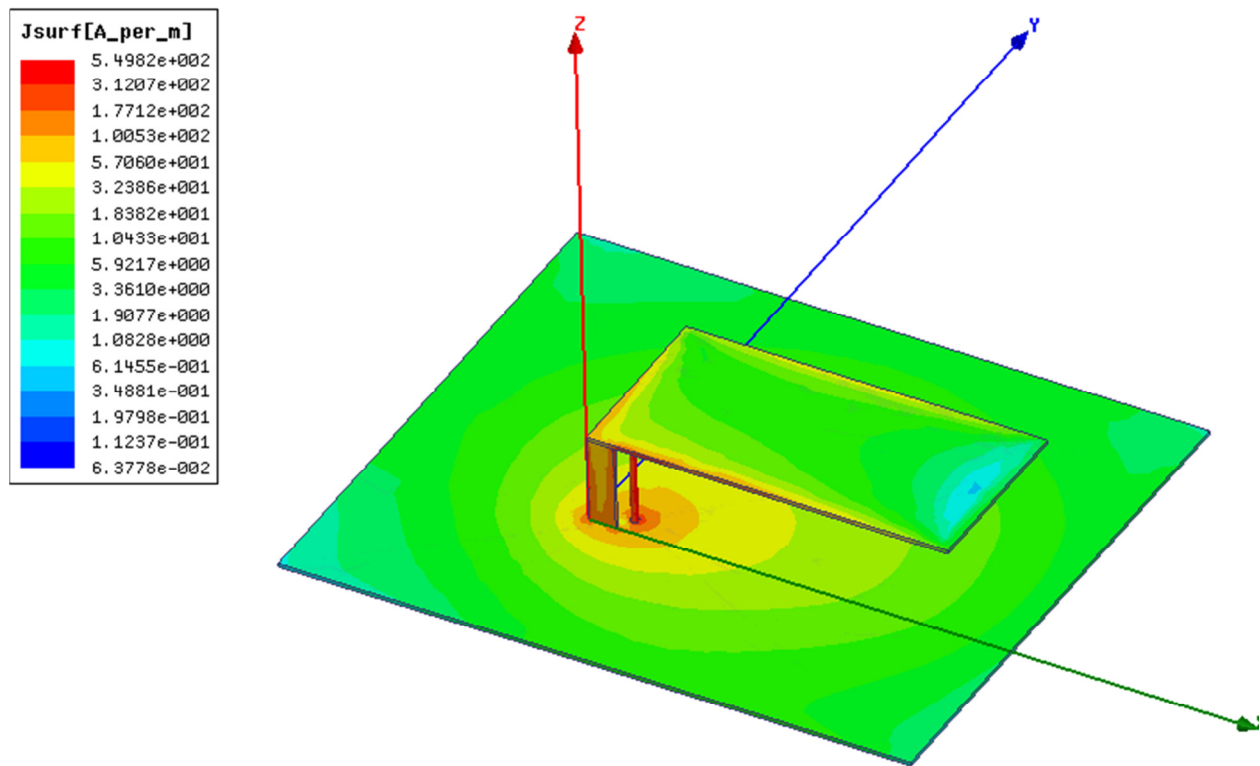


Figure 6.4 Current Density Plot of PIFA Antenna

Strictly speaking, because the nonlinear inductor has both a linear and a nonlinear term, the linear term acts a grounding strip and the nonlinear is used for bandwidth improvement. Substituting the grounding strip with another port now allows the antenna to be simulated as a two port network. The idea here is to load the second port with the nonlinear inductor through cross-communication with an RF circuit simulator.

6.3 Nonlinear Inductor DC Bias Model and Analysis

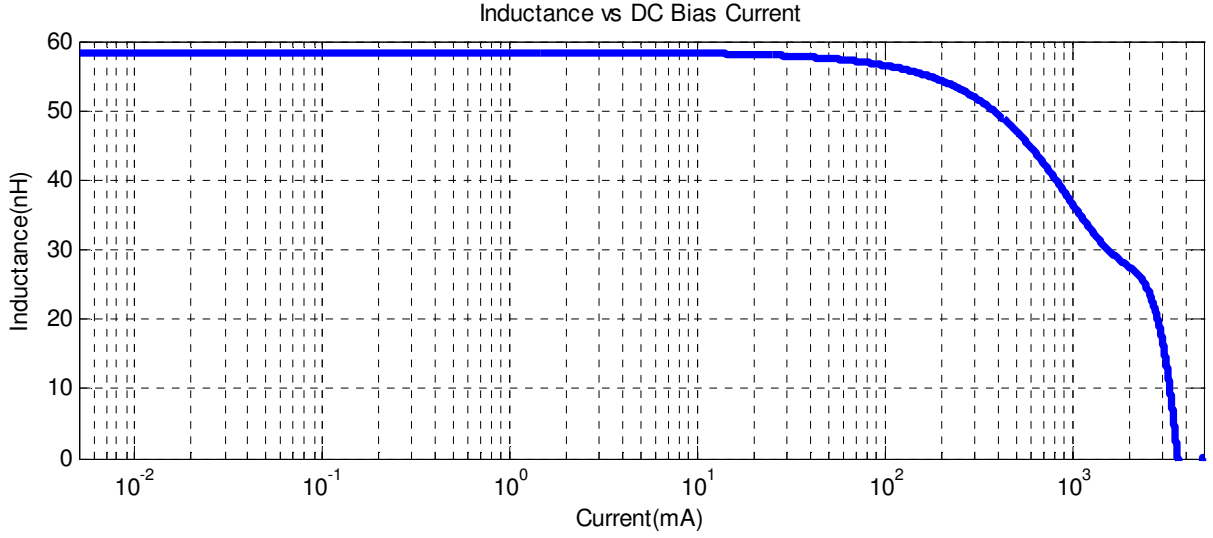


Figure 6.5 Inductance vs. DC Bias Current

The graph in Figure 6.5 shows the inductance of a device as a function of current. The inductance can be modeled as

$$L(i) = L_0 - L_1 i - L_2 i^2 + L_3 i^3 \quad (6.4)$$

For simplicity in derivation and analysis, let's assume L_1 and L_3 are zero. Equation (1) can be further simplified to

$$L(i) = L_0 - L_2 i^2 \quad (6.5)$$

Where the input current i , is defined as the summation of the dc bias current and a variation of the input signal.

$$i = i_{DC} + i_{AC} \sin(\omega_0 t) \quad (6.6)$$

Inserting Equation (6.6) into (6.5), we get:

$$L(i) = L_0 - L_2 (i_{DC} + i_{AC} \sin(\omega_0 t))^2 \quad (6.7)$$

Expanding Equation (6.7), we can now write the inductance as a function of the DC bias current, AC current, frequency and time.

$$\begin{aligned}
 L(i) &= L_0 - L_2 i_{DC}^2 + L_2 2i_{DC} \sin(\omega_0 t) + L_2 i_{AC}^2 \sin^2(\omega_0 t).. \\
 &= L_0 - L_2 i_{DC}^2 + L_2 2i_{DC} \sin(\omega_0 t) + L_2 i_{AC}^2 \left[\frac{1 - \cos(2\omega_0 t)}{2} \right].. \\
 &= \left[L_0 - L_2 i_{DC}^2 + \frac{L_2 i_{AC}^2}{2} \right] + [L_2 2i_{DC}] \sin(\omega_0 t) - \left[\frac{L_2 i_{AC}^2}{2} \right] \cos(2\omega_0 t)
 \end{aligned} \tag{6.8}$$

Observe from the expansion of Equation (6.8) that a nonlinear inductor behaves like a time varying inductor when excited with an AC signal provided that the inductor is biased in the saturation region. In addition, Equation (6.8) also proves that the inductance of the antenna is also highly dependent on the amplitude and frequency of the input signal as well as the DC bias current.

For example, the first term represents an inductance that is function of input current, DC and AC current. The second term is the 1st modulation term or time varying term because it consists of time dependent function of the input frequency. The magnitude for the varying inductance is highly dependent on i_{DC} and L_2 . It is where the DC bias term plays a significant role. The DC current can be controlled or varied to produce different results which is shown later in the chapter.

As a result of the saturation of the inductor, there is generation of other frequency components such as the third term with consists of second order products. The presence of other frequency products leads to lower radiation efficiencies because the signal power is transferred to other frequencies. Consequently, unwanted harmonic signals can be radiated by the antenna. In

addition, the input signal becomes increasing distorted because of the L_2 and i_{AC} term. Therefore nonlinearity is dependent on the input power as well as the nonlinear term L_2 .

6.4 Simulation Results with 1st PIFA Structure

Next, the second port of the PIFA is loaded with a current varying inductor for bandwidth improvement. The nonlinearity in the inductor causes the center frequency of the antenna to shift and also improves the bandwidth in the process. Figure 6.6 shows the reflection coefficient and Table 6.2 shows the summary.

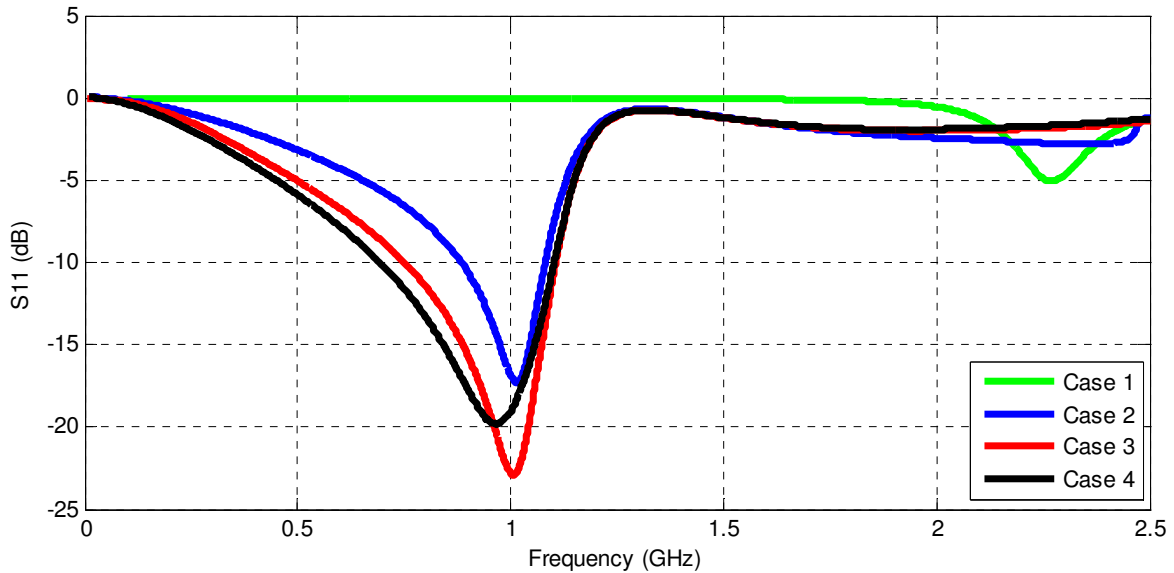


Figure 6.6 Nonlinear Loading on PIFA: results generated using HFSS and ADS.

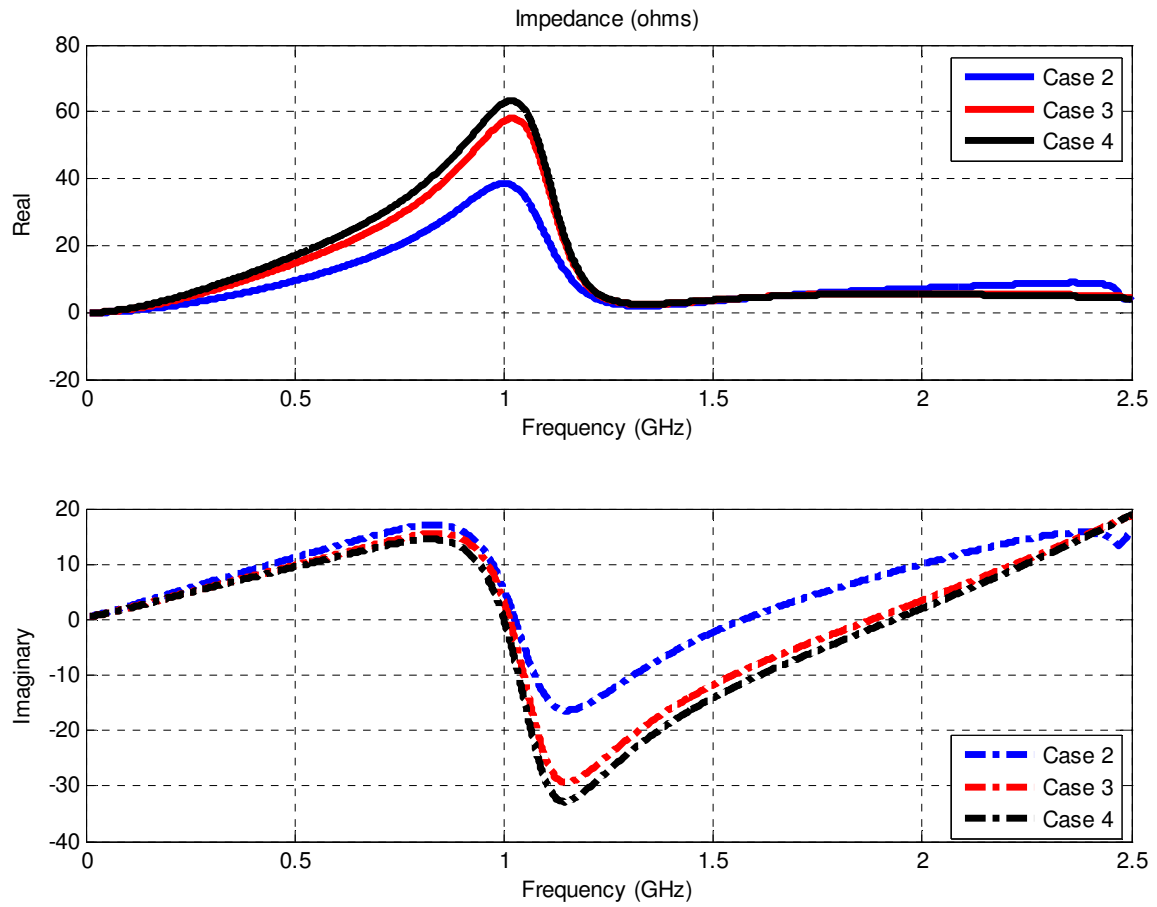


Figure 6.7 Input Impedance of Nonlinear Antenna with different nonlinearities

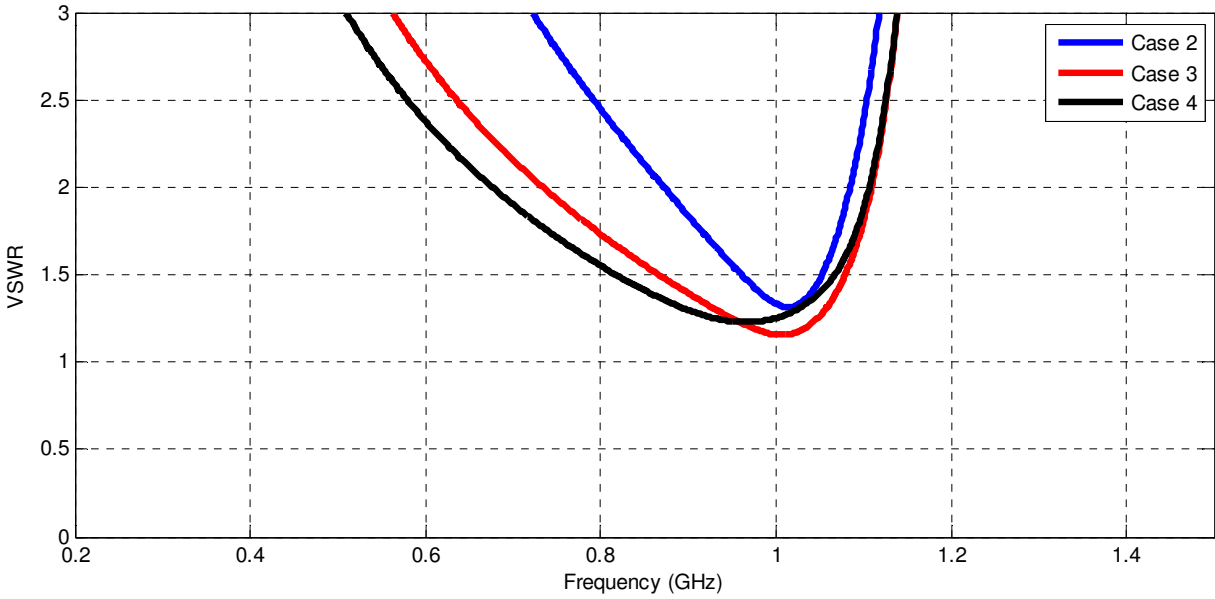


Figure 6.8 Voltage Standing Wave Ratio (VSWR) of Nonlinear Antenna with different nonlinearities

Table 6.2 Summary of Results Generated in Figure 6.6

Case	Type	Source RF Power (dBm)	Source Impedance (Ω)	Inductor ($L = L_0 + L_1i$)	
				L_0	L_1
1	Linear	10	50	0.6nH	0nH
2	Nonlinear	10	50	0.6nH	390nH
3	Nonlinear	10	50	0.6nH	540nH
4	Nonlinear	10	50	0.6nH	590nH

Finally, the results obtained with the nonlinear tuned PIFA is compared with another PIFA antenna centered at 1 GHz. The nonlinear tuned PIFA is able to achieve atleast a 20% bandwidth around the center frequency of 1 GHz. The best case result was around 40% bandwidth as shown in Figure 6.8 and summarized in Table 6.3.

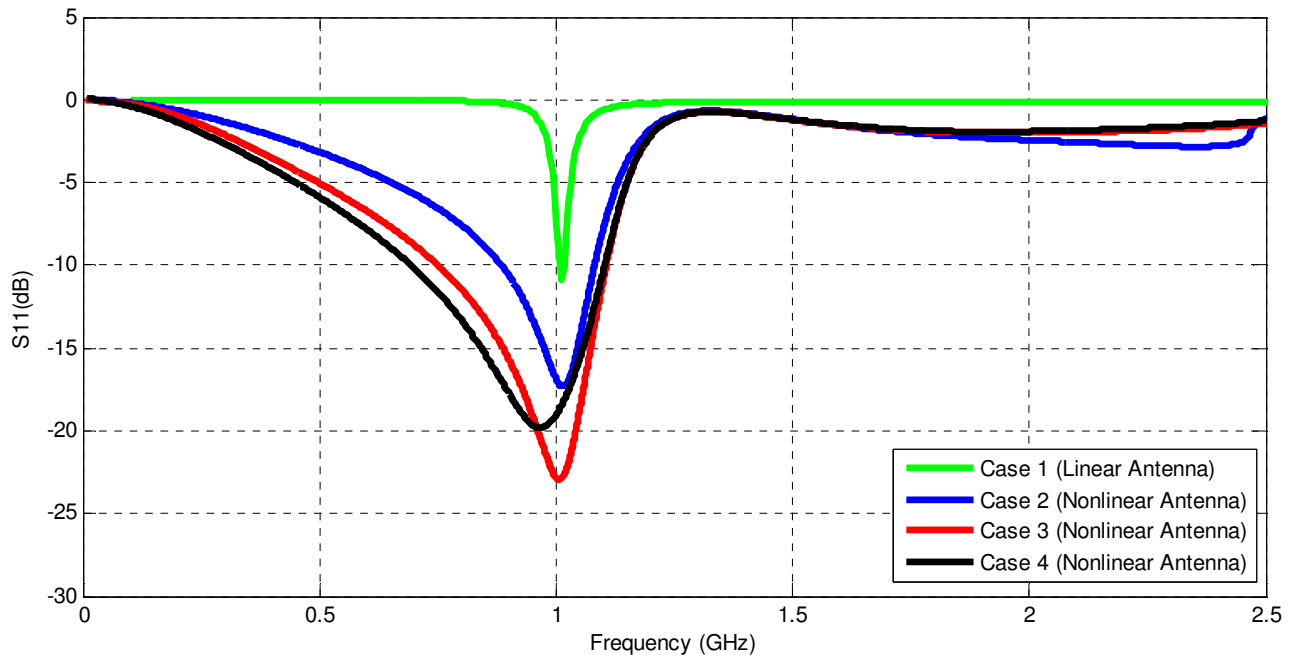


Figure 6.9 Comparison of Linear PIFA vs a Tuned Nonlinear PIFA

Table 6.3 Comparison of Linear PIFA vs a Tuned Nonlinear PIFA

Case	Type	Antenna Dimensions		Center Frequency (GHz)	DC Bias (mA)	Bandwidth (VSWR 2:1)	
		Length	Width			Range	Percentage
1	Linear	50	26	1	0	1.017-1.008 (9 MHz)	0.9%
2	Nonlinear (Tuned)	20	10	1	0	1.08-0.88 (20 MHz)	20.0%
3	Nonlinear (Tuned)	20	10	1	0	1.105-0.751 (354 MHz)	35.4%
4	Nonlinear (Tuned)	20	10	1	0	1.101-0.695 (406 MHz)	40.6%

6.5 Simulation Results with 2nd PIFA Structure

Using the methodology discussed in Section 6.1, another analysis is carried out using second PIFA antenna. The antenna structure without nonlinear loading resonates at 1.4 GHz with a bandwidth of 56 MHz (4%). Figure 6.10 and Figure 6.11 show the reflection coefficient and input impedance respectively.

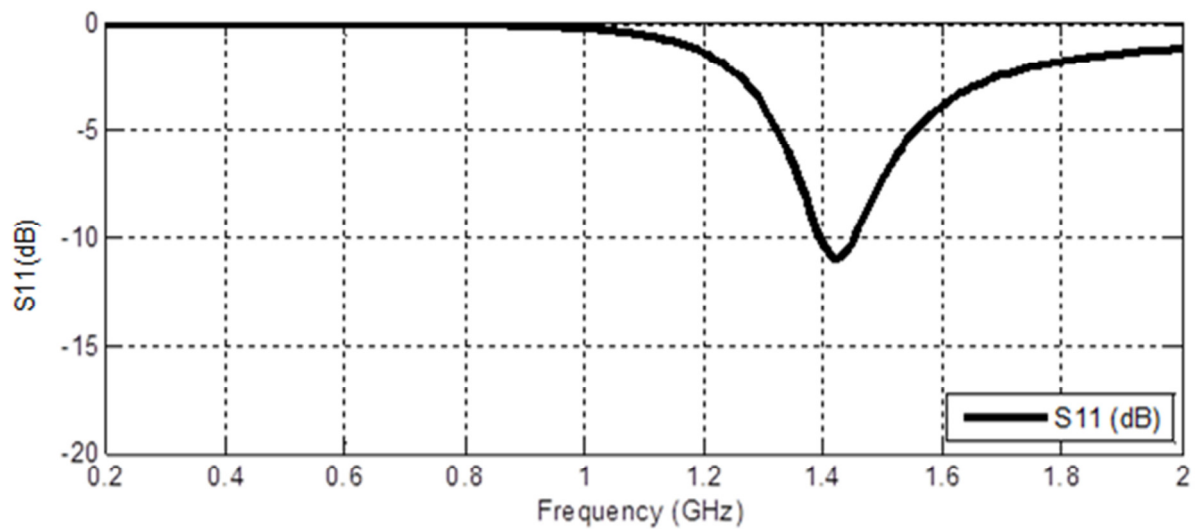


Figure 6.10 Reflection Coefficient (S_{11}) of 1.4 GHz PIFA Structure

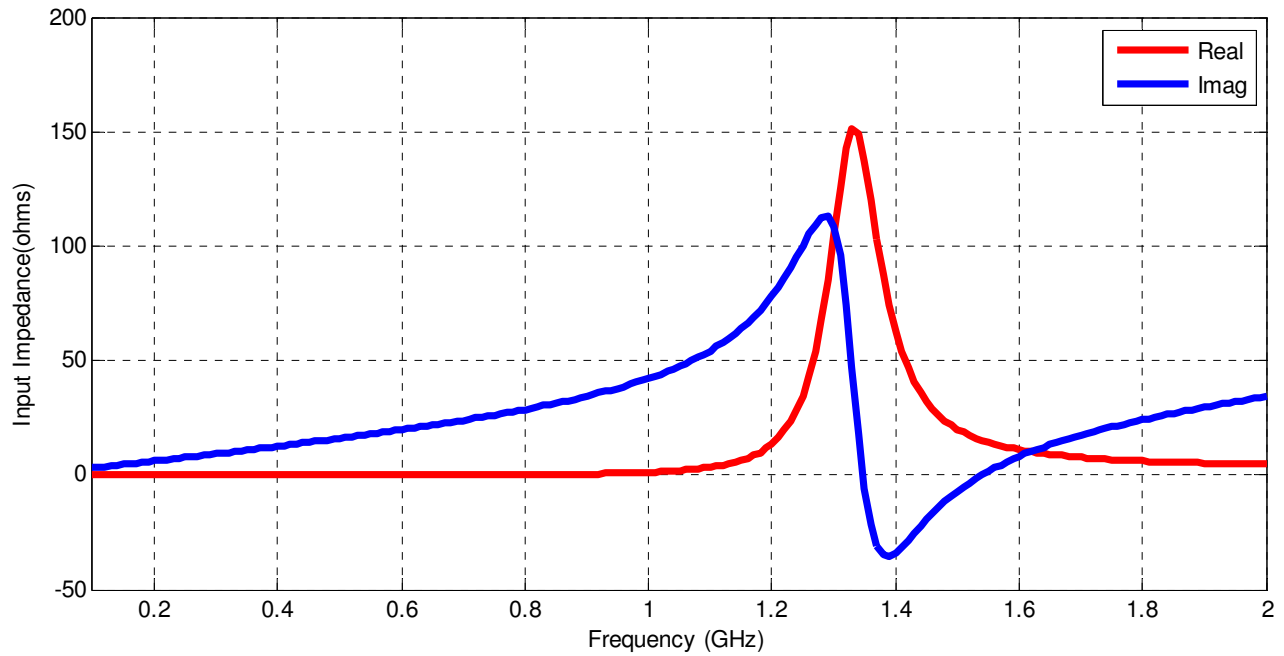


Figure 6.11 Input Impedance of 1.4 GHz PIFA Structure

The shorting pin is replaced with a nonlinear inductor. The nonlinear inductor has a linear as well as a nonlinear term. With the nonlinear term set to zero, the antenna behaves like a linear antenna with a high or low reactance depending on the value of the linear term. Figure 6.12 shows the reflection coefficient of the antenna with a nonlinear load. Case 1 represents the linear case where the nonlinear term is zero as shown in Figure 6.10. The results of Case 2-4 show the S_{11} with different nonlinear terms.

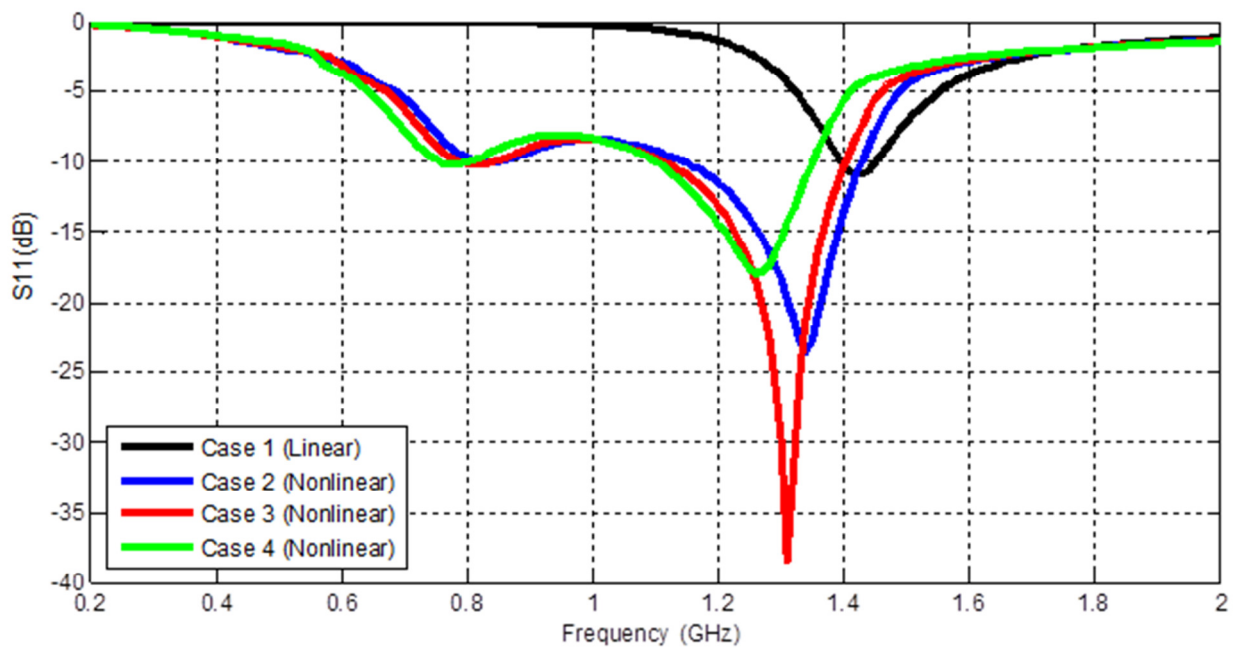


Figure 6.12 Reflection Coefficient of nonlinear loading on 1.4GHz PIFA: results generated using HFSS and ADS

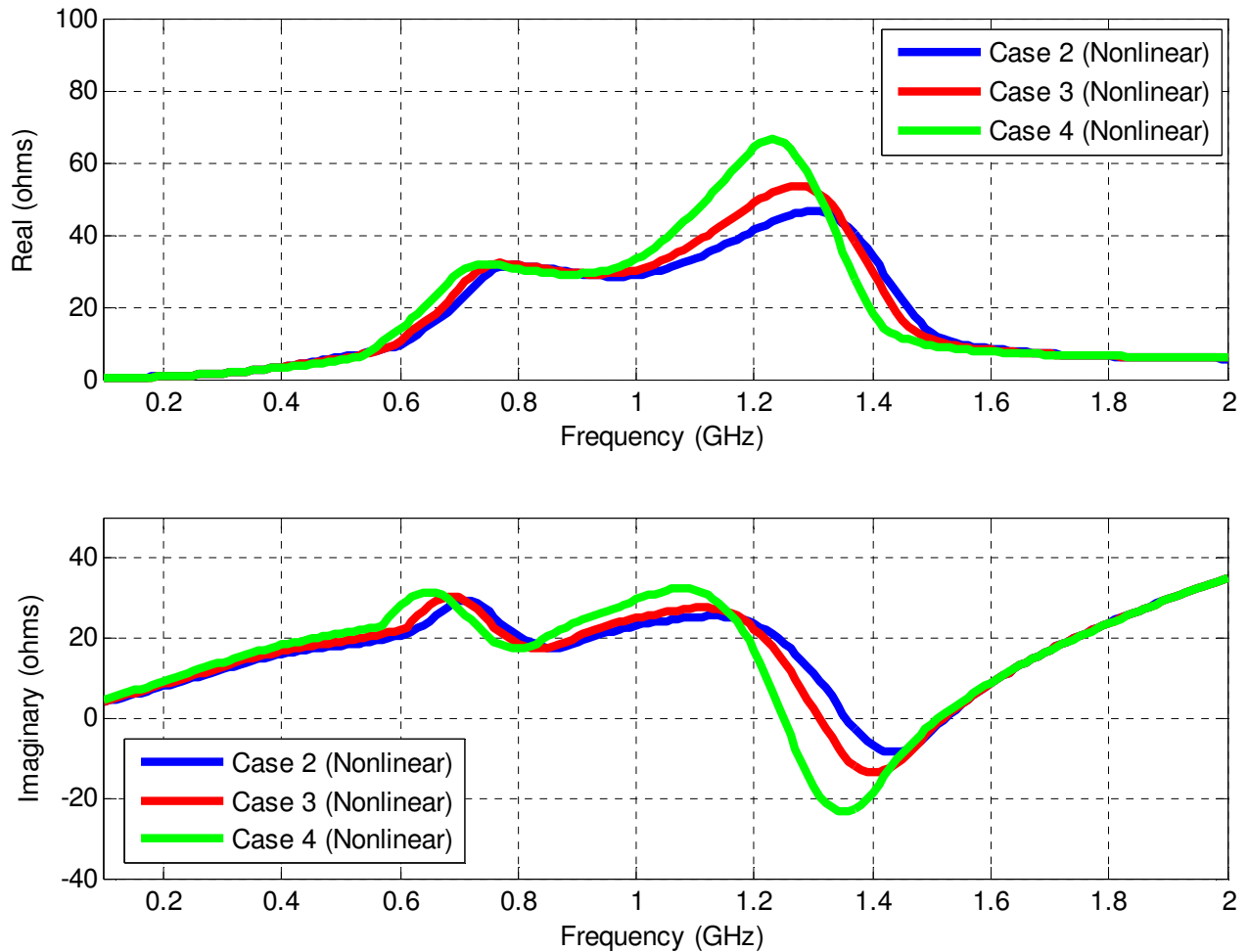


Figure 6.13 Input Impedance of nonlinear loading on 1.4 GHz PIFA: results generated using HFSS and ADS

The bandwidth (VSWR 2:1) of the antenna increases when the nonlinearity in the inductor is varied. When the inductor is completely linearly, the bandwidth is at its minimum as shown by Case 1 in Figure 6.12 and 6.14. Nonlinearity in the inductor reduces the real part of the input impedance as shown in Figure 6.13. Similarity, the reactance of the antenna is reduced which contributes to a wider input impedance bandwidth. In addition, there is a shift in the center frequency when the nonlinearity is varied. Results show an excellent agreement between

numerical and theoretical values generated in Chapter 3 and simulated values using HFSS and ADS.

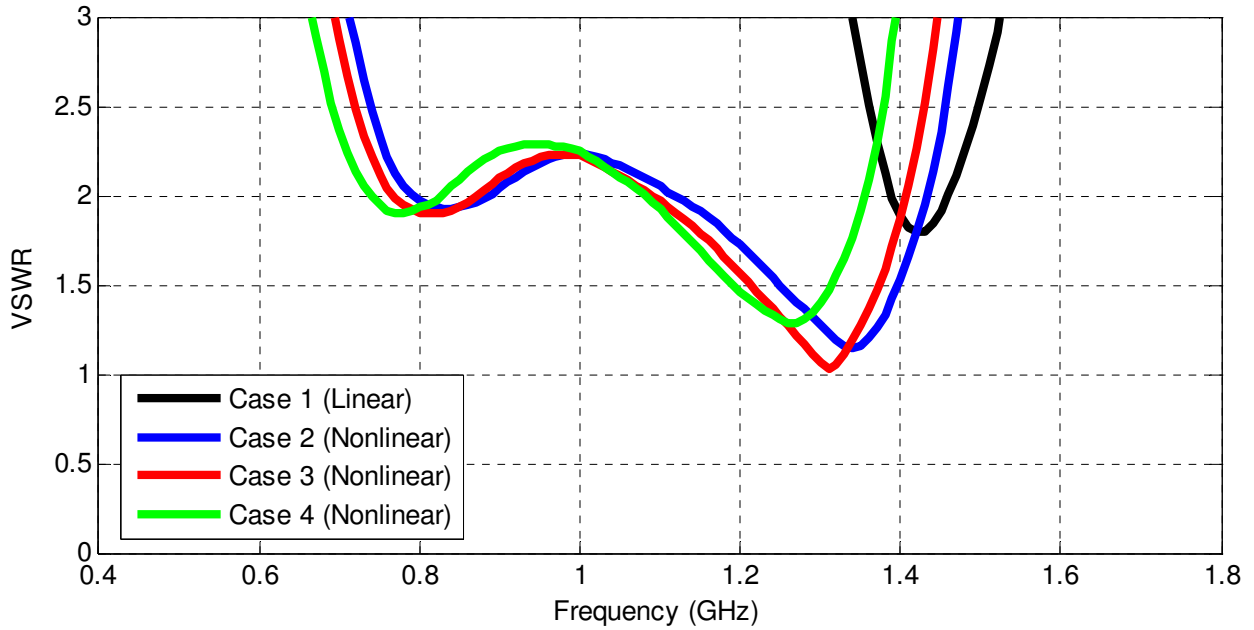


Figure 6.14 VSWR of nonlinear loading on 1.4 GHz PIFA: results generated using HFSS and ADS

Table 6.4 Summary of results generated in Figure 6.14

	Type	Inductor ($L = L_0 - L_2 i^2$)		Center Frequency (GHz)	Current (mA)	Bandwidth (VSWR 2:1)		Efficiency (%)
		L_0	L_2			Range (GHz)/Bandwidth	%	
1	Linear	Shorting Pin		1.42	0	1.390-1.46 (70 MHz)	4.9	90.5
2	Nonlinear	15.4nH	1uH	1.34	117.02	1.12-1.435 (315 MHz)	23.5	44
3	Nonlinear	15.4nH	1uH	1.31	115.40	1.09-1.405 (315MHz)	24	26
4	Nonlinear	15.4nH	1uH	1.26	112.63	1.08-1.355 (275 MHz)	21.8	26.6

A summary of the results for the second PIFA antenna is presented in Table 6.4. While there is an input impedance bandwidth improvement with nonlinearity, the antenna's efficiency suffers.

Because nonlinearity in the inductor generates harmonics, a portion of the input power dissipates

at harmonic frequencies. Figure 6.15 shows the input power and radiated power at the harmonics of the fundamental frequency and Section 6.6 discusses these concerns as well as others.

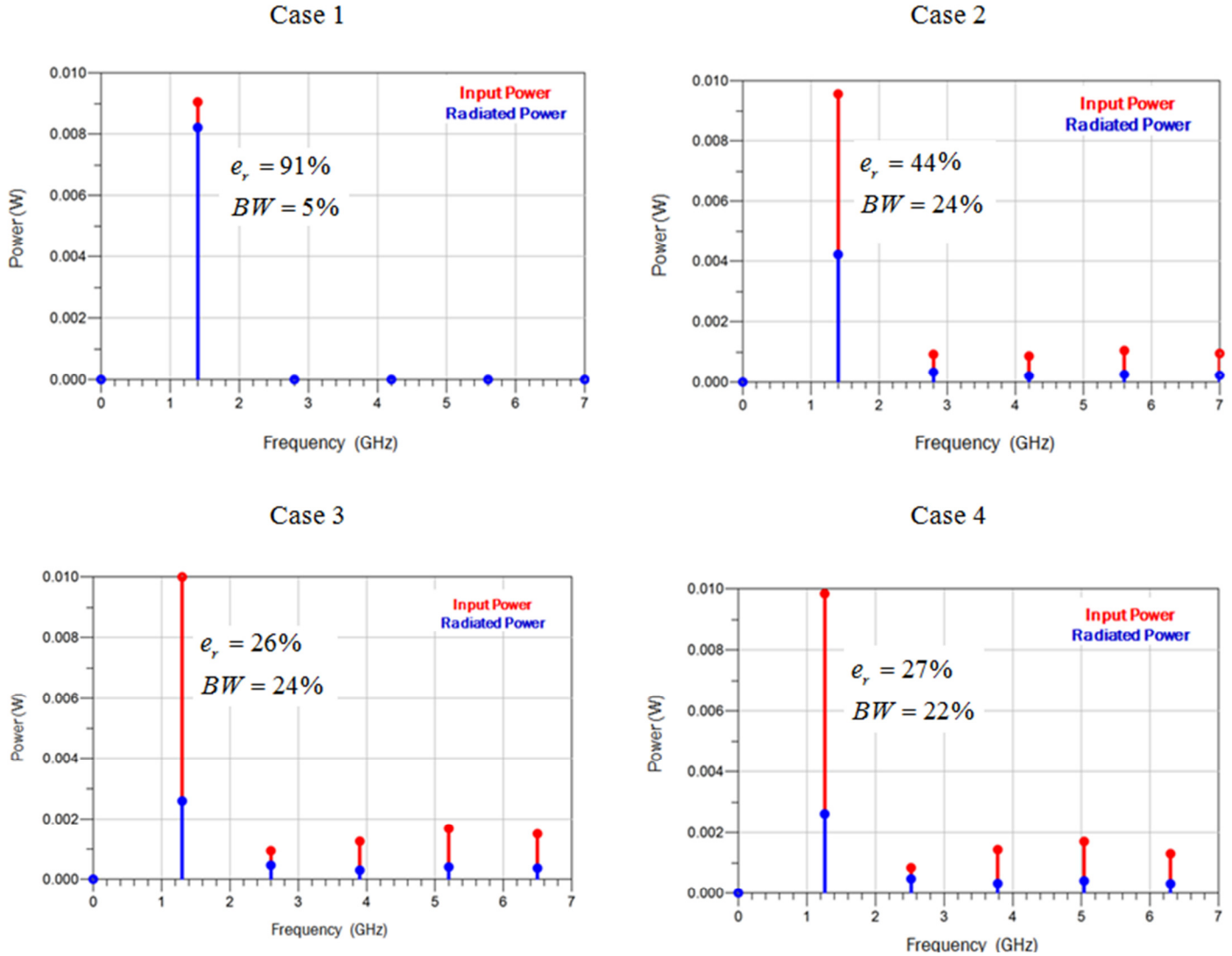


Figure 6.15 Input Power and Radiated Power at Harmonics of the Fundamental Frequency

6.6 Concerns using Nonlinearity

Loss in the Harmonics Many nonlinear devices such as diodes and transistors utilize their nonlinearity for functions such as amplification, detection and frequency conversion [3]. Much

like diodes and transistors, it is possible for the nonlinearity in the inductor to generate harmonics and spurious frequencies that inevitably lead to losses in the antenna. Driving the nonlinearity in the circuit at high RF powers will generate unwanted harmonics. More work has to be done in this area to effectively study and measure harmonic losses in the system.

Radiation efficiency Radiation efficiency describes how much of input power is actually radiated by the antenna. An actual nonlinear device exhibits resistive loss due to non-perfect materials. With resistive loss in the components, the radiation efficiency of the antenna is reduced.

Waveform Distortion Nonlinearity in the antenna will cause the RF input waveform to be distorted. Therefore, the information transmitted to the antenna could be distorted before it is radiated. In addition to noise, the received signal received from a nonlinear antenna could have a distortion. Since the distortion is caused by harmonics, a filter can be used to recover the original signal.

References

- [1] S. Maas. (2003). *Nonlinear Microwave and RF Circuits (2nd ed.) [Online]*. Available: www.artechhouse.com

- [2] Agilent Technologies. (2004). *Large-Signal S-Parameters Simulation [Online]*. Available: http://www.ece.uci.edu/eceware/ads_docs/pdf/cktsimlssp.pdf

- [3] M. E. Hines, “The Virtues of Nonlinearity – Detection, Frequency Conversion, Parametric Application and Harmonic Generation,” *IEEE Trans. Microwave Theory and Techniques*, vol. MTT-32, pp. 1097-1104, September 1984.

Chapter 7 Conclusions

A new concept of loading an antenna with a nonlinear inductor for bandwidth improvement is presented in this thesis. Initial simulations on a narrowband planar inverted-F antenna show bandwidth enhancement. This chapter presents a summary of the important points and theories in the thesis. It also discusses contributions to the antenna world and future work.

7.1 Summary

Chapter 2 starts by with a history of mobile communication systems and multiple-resonate antennas. Fundamental properties of small antennas such as gain, directivity, input impedance and efficiency are also reviewed. The fundamental limits of antennas relating to quality factor and bandwidth are discussed and the possibility of breaking Chu's quality factor criteria using nonlinearity.

Chapter 3 lays the foundation for using nonlinearity to improve a narrowband antenna. A parallel RLC circuit model is used for the antenna and a shunt nonlinear inductor is attached to it.

The frequency response of the input impedance is calculated using the Fourier transform along with the 4th order Runge-Kutta numerical method. The results validate the possibility of using nonlinear elements for antenna input impedance bandwidth improvement.

With the foundation set, Chapter 4 covered several candidate narrowband antennas. Antennas such as the Inverted-L and Inverted-F Antenna were considered on a theoretical level. Based on the structure of the nonlinear inductor, the most suitable choice was the Planar Inverted F antenna. Chapter 5 deals with the designing of a linear PIFA antenna

Chapter 6 presents a nonlinear PIFA antenna with an improved input impedance bandwidth. It illustrates the modifications performed on the linear PIFA Antenna presented in Chapter 5 to make it suitable for a nonlinear inductor. It also discusses the setup used to calculate the input impedance and reflection coefficient. The results are presented and compared with a tradition narrowband PIFA antenna.

7.2 Contributions

The results presented in Chapter 6 show that an antenna input impedance bandwidth can be improved by loading a nonlinear inductor to it. The linear term of the inductor controls the tuning range of the inductor while the nonlinear enhances the bandwidth. In addition, the antenna can also be miniaturized by reducing the size and then tuning to a lower resonant frequency. Although more work has to be done, preliminary work shows the antenna input impedance bandwidth can be enhanced while reducing its size as well.

7.3 Future Work

With initial analysis showing that nonlinearity in the antenna does improve the input impedance bandwidth, the next step to prototype a low loss nonlinear inductor. This nonlinear inductor will be attached to the Planar Inverted-F antenna for bandwidth improvement. Measurements on the reflection coefficient and radiation patterns could be done to further validate the simulation results. In addition, other nonlinear devices could be attached to the antenna to investigate bandwidth improvement.